1   **Tropospheric aerosol hygroscopicity measurements in China**

2   Chao Peng,[1] Yu Wang,[2] Zhijun Wu,[2] Lanxiadi Chen,[1,6] Ru-Jin Huang,[3] Weigang Wang,[4] Zhe

3   Wang,[5] Weiwei Hu,[1] Guohua Zhang,[1] Maofa Ge,[4,6,7] Min Hu,[2] Xinming Wang,[1,6,7] Mingjin

4   Tang,[1,6,7,*]

5

6   1 State Key Laboratory of Organic Geochemistry, Guangdong Key Laboratory of Environmental Protection and

7   Resources Utilization, and Guangdong-Hong Kong-Macao Joint Laboratory for Environmental Pollution and

8   Control, Guangzhou Institute of Geochemistry, Chinese Academy of Sciences, Guangzhou 510640, China

9   [2] State Key Joint Laboratory of Environmental Simulation and Pollution Control, College of Environmental

10   Sciences and Engineering, Peking University, Beijing 100871, China

11   [3] State Key Laboratory of Loess and Quaternary Geology, Center for Excellence in Quaternary Science and

12   Global Change, and Key Laboratory of Aerosol Chemistry and Physics, Institute of Earth Environment,

13   Chinese Academy of Sciences, 710061 Xi'an, China

14   [4] State Key Laboratory for Structural Chemistry of Unstable and Stable Species, Beijing National Laboratory

15   for Molecular Sciences (BNLMS), CAS Research/Education Center for Excellence in Molecular Sciences,

16   Institute of Chemistry, Chinese Academy of Sciences, Beijing 100190, China

17   [5] Division of Environment and Sustainability, The Hong Kong University of Science and Technology, Hong

18   Kong, China

19   [6] University of Chinese Academy of Sciences, Beijing 100049, China

20   [7] Center for Excellence in Regional Atmospheric Environment, Institute of Urban Environment, Chinese

21   Academy of Sciences, Xiamen 361021, China

22

23   * Correspondence: Mingjin Tang (mingjintang@gig.ac.cn)

24

25

Atmospheric
Chemistry
and Physics
Discussions

26 **Abstract**

27   Hygroscopicity largely determines phase state, chemical reactivity, optical properties and

28 cloud nucleation activities of aerosol particles, thus significantly affecting their impacts on

29 visibility, atmospheric chemistry and climate. In the last twenty years a large number of field

30 studies have investigated hygroscopicity of tropospheric aerosols in China under sub- and super-

31 saturated conditions. Aerosol hygroscopicity measurements in China are reviewed in this paper: 1)

32 a comprehensive summary and critical discussion of aerosol hygroscopicity measurements in

33 China is provided; 2) available measurement data are compiled and presented under a consistent

34 framework to enhance their accessibility and usability; 3) current knowledge gaps are identified,

35 and an outlook which could serve as guidelines for planning future research is also proposed.

36

37

1 Introduction

In the last few decades, rapid industrial, economic and social developments in China have caused large emissions of gaseous and particulate pollutants into the troposphere (Li et al., 2017a), where they are mixed with gases and aerosols from natural sources. Under unfavourable meteorological conditions (i.e. when air is stagnant and stable), severe air pollution occurs, due to accumulation of primary pollutants and more importantly, formation of secondary pollutants (Zhu et al., 2011; He et al., 2014; Zhang et al., 2015; An et al., 2019; Lu et al., 2019; Zhang et al., 2019c). During severe air pollution events, $PM_{2.5}$ could exceed a few hundred μg m^{-3} (Guo et al., 2014; Huang et al., 2014) and O_3 could reach up to >200 ppbv (Wang et al., 2017a). The concept of air pollution complex has been proposed to describe the complexity of air pollution in China, characterized by complex sources and complex interactions of a myriad of gaseous and particulate pollutants (Zhu et al., 2011; Lu et al., 2019; Chu et al., 2020). Thanks to the implementation of effective air pollution control measures, substantial decrease in $PM_{2.5}$ has occurred nationwide in the last several years (Zhang et al., 2019b); however, slight but significant increase in O_3 has been observed in many regions during the same period (Li et al., 2019a; Lu et al., 2020), revealing the complexity and difficulty in synergistic control of $PM_{2.5}$ and O_3.

Hygroscopicity, one of the most important physicochemical properties of aerosols, determines the amount of water associated with aerosol particles under ambient conditions (mainly relative humidity, and temperature to a less extent) and significantly affects their environmental and climatic impacts (Kreidenweis and Asa-Awuku, 2014; Tang et al., 2019). Hygroscopicity is referred to hygroscopic properties under subsaturated conditions from a specific view, while from a general view, it is referred to both hygroscopic properties under subsaturated conditions and cloud condensation nucleation (CCN) activities under supersaturated conditions. Due to their

61   hygroscopicity, aerosol particles will take up water (i.e. hygroscopic growth) and lead to increase

62   in particle mass and size (Kreidenweis and Asa-Awuku, 2014; Tang et al., 2016; Wu et al., 2018b;

63   Tang et al., 2019). Therefore, hygroscopicity largely determines optical properties of aerosols and

64   as a result their impacts on visibility and direct radiative forcing under subsaturated conditions

65   (Titos et al., 2016; Zhao et al., 2019); on the other hand, hygroscopicity is also closely linked to

66   CCN activities of aerosols and thus their abilities to from cloud droplets under supersaturated

67   conditions (Kreidenweis and Asa-Awuku, 2014; Farmer et al., 2015; Tang et al., 2016), thereby

68   having important implications for their indirect radiative forcing (Dusek et al., 2006; McFiggans

69   et al., 2006; Farmer et al., 2015). Furthermore, hygroscopicity determines aerosol liquid water

70   content (ALWC) and thus phase state, acidity and chemical reactivities of aerosols (Bertram and

71   Thornton, 2009; Liu et al., 2017; Tang et al., 2017; Wu et al., 2018b), playing critical roles in

72   secondary aerosol formation as well as removal and production of trace gases. In addition,

73   hygroscopic growth measurements can provide valuable insights into mixing states of aerosols

74   (Swietlicki et al., 2008; Riemer et al., 2019). Due to its importance, tropospheric aerosol

75   hygroscopicity has been investigated in China by a number of field studies in the last 10-20 years,

76   as reviewed in this paper.

77   Swietlicki et al. (Swietlicki et al., 2008) summarized and analyzed hygroscopic properties of

78   ambient aerosols measured using H-TDMA (Hygroscopic Tandem Differential Mobility Analyser)

79   prior to September 2007, when ambient aerosol hygroscopicity was seldom explored in China. The

80   effects of hygroscopicity on aerosol light scattering have been reviewed and summarized on the

81   global scale (Titos et al., 2016; Burgos et al., 2019), and a very recent paper also briefly

82   summarizes aerosol light scattering enhancement studies in China (Zhao et al., 2019). A book

83   chapter (Kreidenweis and Asa-Awuku, 2014) discussed in brief hygroscopic growth and light

Atmospheric
Chemistry
and Physics
Discussions

84   scattering enhancement of ambient aerosols, but only a few measurements conducted in China

85   were included. In addition, a recent paper (Tang et al., 2019) has reviewed aerosol hygroscopicity

86   measurement techniques. However, aerosol hygroscopicity measurements in China have not been

87   reviewed yet.

88   In this paper we provide a comprehensive review of hygroscopic properties of ambient aerosols

89   measured using H-TDMA in China; in addition, CCN activities of tropospheric aerosols measured

90   in China are also reviewed and discussed. Via using the single hygroscopicity parameter (κ), we

91   attempt to reconcile hygroscopic properties examined at <100% RH (relative humidity) with CCN

92   activities measured at >100% RH. A number of studies measured light scattering enhancement

93   factors, f(RH), of ambient aerosols in China (Zhao et al., 2019), but most of these studies are not

94   included herein for two reasons: 1) f(RH) measurements in China have been reviewed in brief very

95   recently (Zhao et al., 2019); 2) it is not trivial to convert measured f(RH) to growth factors or κ

96   values (Kreidenweis and Asa-Awuku, 2014). Nevertheless, we note that some methods have been

97   proposed to convert measured f(RH) to κ (Kuang et al., 2017; Kuang et al., 2018). Single particle

98   techniques were employed to investigate hygroscopic properties of tropospheric aerosols (Li et al.,

99   2016); however, as numbers of particles examined in single particle studies are usually too limited

100   to provide enough information for the overall aerosol hygroscopicity, these studies are not

101   discussed herein. Although not covered in this review, remote sensing techniques can also be used

102   to retrieve aerosol hygroscopicity in the troposphere (Lv et al., 2017; Bedoya-Velásquez et al.,

103   2018; Tang et al., 2019; Dawson et al., 2020).

104   The first goal of this paper is to provide a comprehensive overview of hygroscopic properties

105   and CCN activities of tropospheric aerosols in China via reviewing previous field studies. The

106   second goal is to compile and present measurement data (as compiled in Tables S1-S5) reported

107   by previous work using a consistent framework (i.e. via using the single hygroscopicity parameter)

108   to enhance their accessibility and usability. The third goal, perhaps more importantly, is to identify

109   knowledge gaps in this field and then to provide an outlook which can serve as practical guidelines

110   for planning future research. In this paper, Section 2 describes the methodology adopted in this

111   paper to analyse and review previous studies, and previous measurements of hygroscopic

112   properties and CCN activities of tropospheric aerosols in China are reviewed and discussed in

113   Sections 3 and 4. In the end, Section 5 outlines knowledge gaps and research perspectives.

114   **2 Methodology**

115   **2.1 Hygroscopic properties**

116   H-TDMA instruments, initially developed ~40 years ago (Liu et al., 1978; McMurry et al.,

117   1983; Rader and McMurry, 1986; McMurry and Stolzenburg, 1989), have been widely used in

118   field and laboratory studies (Kreidenweis et al., 2005; Svenningsson et al., 2006; Gysel et al., 2007;

119   Sjogren et al., 2008; Swietlicki et al., 2008; Duplissy et al., 2009; Asmi et al., 2010; Liu et al.,

120   2011; Wu et al., 2011; Kreidenweis and Asa-Awuku, 2014; Zieger et al., 2017; Tang et al., 2019).

121   Technical details of H-TMDA measurements, including operation principles, data analysis and etc.,

122   have been detailed in a review paper (Swietlicki et al., 2008). In brief, an aerosol flow, dried to

123   <20% RH, is passed through an aerosol neutralizer and the first DMA (Differential Mobility

124   Analyzer) to produce quasi-monodisperse aerosols with a given mobility diameter; after that, the

125   aerosol flow is delivered through a humidifier to be humidified to a given RH, and subsequently

126   aerosol size distributions are measured using the second DMA coupled with a CPC (Condensation

127   Particle Counter). The hygroscopic growth factor, GF, is defined as the ratio of the aerosol mobility

128   diameter at a given RH to that at dry conditions. As aerosol particles at a given size may have

129   different hygroscopic properties and thus display different GF values at a given RH, probability

130   distribution functions of GF (i.e. number fractions of aerosol particles at each GF) have also been

131   reported in some studies.

132   The measured distribution functions of GF are usually smoothed and skewed due to several

133   reasons, e.g., the finite width of the DMA's transfer function, and several TDMA inversion

134   algorithms have been proposed to convert the H-TDMA raw data to the probability density

135   function of GF (Stolzenburg and McMurry, 1988; Stratmann et al., 1997; Voutilainen et al., 2000;

136   Cocker et al., 2001; Cubison et al., 2005; Gysel et al., 2009). The algorithm developed by Gysel

137   et al., TDMAinv, is currently the most widely used one. Errors and uncertainties of H-TDMA data

138   can come from several sources, including RH and temperature variability, electrical mobility

139   classification, particle non-equilibrium in the second DMA, and etc. Swietlicki et al. (Swietlicki

140   et al., 2008) comprehensively discussed the sources and magnitudes of these errors and how they

141   can be reduced or minimized. In addition, guidelines used for H-TDMA measurements, including

142   instrumental design, calibration, validation and operation as well as data analysis, have been

143   recommended in literature (Duplissy et al., 2009; Massling et al., 2011).

144   H-TDMA measurements of ambient aerosols were typically conducted for a few different

145   particles diameters at a given relative humidity (RH); most measurements were carried out at 90%

146   RH, though some studies also reported growth factors (GF) at other RH. To facilitate comparison

147   of GF reported at different RH, we convert GF measured at a given RH to κ using Eqs. (1-2)

148   (Petters and Kreidenweis, 2007; Tang et al., 2016):

149    $\kappa = (\mathrm{GF}^3 - 1)(\frac{B}{RH} - 1)$ (1)

150    $B = \exp\left(\frac{A}{d_0 \cdot GF}\right)$ (2)

151   where d_0 is the dry particle diameter; A, which describes the Kelvin effects, is equal to 2.1 nm at

152   298.15 K if the surface tension is assumed to be the same as water (0.072 J m^{-2}) (Petters and

153   Kreidenweis, 2007; Tang et al., 2016). Converting GF to κ also facilitates comparison between

154   hygroscopic properties and CCN activities. For a few studies which reported GF at different RH,

155   we focus GF measured at 90% RH; if the data at 90% are not available, we then choose

156   measurements at the RH closest to 90%.

157   To further facilitate comparison between different measurements, Swietlicki et al. (Swietlicki

158   et al., 2008) classified aerosol hygroscopicity into four groups according to their GF at 90% RH.

159   This methodology was adopted by Ye et al. (Ye et al., 2013) who reported aerosol hygroscopic

160   growth measurements in Shanghai. Nevertheless, Ye et al. (Ye et al., 2013) classified aerosol

161   particles into three modes (instead of four), and the criterions used are slightly different from

162   Swietlicki et al. (Swietlicki et al., 2008). Here we adopt the method proposed by Ye et al. (Ye et

163   al., 2013), who classified aerosol hygroscopicity into three modes, including the nearly-

164   hydrophobic (NH, $\kappa<0.1$), the less-hygroscopic (LH, $0.1<\kappa<0.0.25$) and the more-hygroscopic

165   (MH, $\kappa>0.0.25$) modes. However, here a few further statements are necessary. First, terminologies

166   used differ in previous studies for aerosol hygroscopicity modes. For example, bimodal aerosol

167   hygroscopicity was frequently observed in China (as discussed in Section 3), and the nearly-

168   hydrophobic mode defined by Ye et al. (Ye et al., 2013) was called the less-hygroscopic mode or

169   the low-hygroscopic mode in several studies. Second, actual aerosol hygroscopicity in the

170   troposphere may not perfectly fit into one of the three modes defined by Ye et al. (Ye et al., 2013).

171   **2.2 CCN activities**

172   A variety of instruments have been developed to measure CCN number concentrations

173   (Twomey, 1963; Sinnarwalla and Alofs, 1973; Fukuta and Saxena, 1979; Hudson, 1989; Ji et al.,

Atmospheric
Chemistry
and Physics
Discussions
Open Access
EGU

174   1998; Chuang et al., 2000; McMurry, 2000; Nenes et al., 2001; Otto et al., 2002; VanReken et al.,

175   2004; Roberts and Nenes, 2005; Frank et al., 2007; Kreidenweis and Asa-Awuku, 2014). Currently

176   the most widely used one is the continuous-flow streamwise thermal gradient CCN counter based

177   on the design of Roberts and Nenes (Roberts and Nenes, 2005; Lance et al., 2006) and

178   commercialized by Droplet Measurement Technologies, and mode details of this instrument can

179   be found elsewhere (Roberts and Nenes, 2005; Lance et al., 2006).

180   Measurements of size-resolved CCN activities have been discussed in a number of previous

181   studies (Lance et al., 2006; Frank et al., 2007; Petters et al., 2007; Rose et al., 2008; Good et al.,

182   2010; Moore et al., 2010; Rose et al., 2010; Bougiatioti et al., 2011). In many studies, an aerosol

183   flow sampled from the ambient air, after dried to <20% RH, is passed through an aerosol

184   neutralizer and then a DMA to produce quasi-monodisperse aerosols. The aerosol flow is

185   subsequently split into two flows; one flow is sampled into a CCN counter to measure number

186   concentrations of cloud condensation nuclei ([CCN]), and the other one is sampled into a CPC to

187   measure number concentrations of condensation nuclei ([CN]). At a given supersaturation,

188   activation fractions ([CCN]/[CN]) are measured as a function of particle diameter (selected using

189   the DMA) and then fitted by an activation curve to determine the activation diameter at which the

190   activation fraction is equal to 0.5 (Snider et al., 2006; Rose et al., 2008; Sullivan et al., 2009;

191   Bougiatioti et al., 2011; Cerully et al., 2011), and activation fractions can be measured at one or

192   more supersaturation as a function of particle diameter. Methods used for instrument calibration

193   and data correction, which can be found in literature (Frank et al., 2007; Petters et al., 2007; Rose

194   et al., 2008; King et al., 2009; Petters et al., 2009; Moore et al., 2010), are not discussed herein.

195   Furthermore, κ can be derived from the determined activation diameter at a given supersaturation

196   (Petters and Kreidenweis, 2007).

197   Maximum activation fractions may not approach one for ambient aerosols, and generally two

198   methods have been used to fit the data. If the maximum activation fraction of the fitted activation

199   curve is not fixed (three-parameter fit), the derived activation diameter (d_a) and single

200   hygroscopicity parameter (κ_a) describe the average properties of activated particles; if it is forced

201   to be 1 (two-parameter fit), the derived activation diameter (d_t) and single hygroscopicity

202   parameter (κ_t) describe the overall aerosol properties (Rose et al., 2010). For aerosols with bimodal

203   hygroscopicity distribution, κ_a is comparable to the κ determined using H-TDMA for the more-

204   hygroscopic mode, while κ_t is comparable to the average κ for the two modes. In addition to d_a and

205   d_t, the apparent cut-off diameter (above which [CN] is equal to [CCN] at a given supersaturation.),

206   d_{cut} (and thus κ_{cut}), can be determined if it is assumed that particles at each size are internally mixed

207   and that larger particles are activated first (Rose et al., 2010; Hung et al., 2014). The determination

208   of d_{cut} does not required size-resolved activation fractions, but needs the overall activation fractions

209   and aerosol number size distribution (Burkart et al., 2011; Hung et al., 2014). Our review paper is

210   focused on κ_a and to a less extent κ_t, and only discusses κ_{cut} when neither κ_a nor κ_t was reported.

211   In addition, [CCN] and [CCN]/[CN] were also measured at one or more supersaturation in

212   Tianjin (Deng et al., 2011; Yang et al., 2012; Zhang et al., 2012), Zhangjiakou (Hebei) (Lu and

213   Guo, 2012), Shijiazhuang (Hebei) (Lu and Guo, 2012), Xingtai (Hebei) (Wang et al., 2018b),

214   Qingdao (Li et al., 2015a), Shanghai (Leng et al., 2013; Leng et al., 2014), Guangzhou (Duan et

215   al., 2017; Duan et al., 2018) and Mt. Huang (Fang et al., 2016), as well as over marginal seas of

216   China (Zhu et al., 2019; Gao et al., 2020) and northwestern Pacific (Wang et al., 2019a; Zhu et al.,

217   2019). As these studies did not carry out size-resolved measurements and thus did not report

218   critical diameters or κ, they are not further discussed herein.

3 Hygroscopic growth

A number of aerosol hygroscopic growth measurements have been carried out in China since 2001 using H-TDMA (or very similar instruments). Most of these measurements were performed in three regions with severe air pollution, including the North China Plain (NCP), Yangtze River Delta (YRD) and Pearl River Delta (PRD), and these studies are discussed in Sections 3.1-3.3. In addition, as discussed in Section 3.4, several measurements were also conducted at other locations in the east or south China.

3.1 North China plain (NCP)

The North China Plain is a heavily polluted region where many aerosol hygroscopic growth measurements were conducted, and as summarized in Table S1. In this section we review the measurements carried out at urban sites in Beijing (Section 3.1.1), rural sites in Beijing (Section 3.1.2), other urban/suburban sites (Section 3.1.3) and other rural sites (Section 3.1.4).

3.1.1 Urban sites in Beijing

Aerosol hygroscopic growth has been measured at three urban sites in Beijing, including the PKU site, the IAP site, and the CAMS site.

PKU site: The PKU site is located on the campus of Peking University (39°59'20"N, 116°18'26"E), which is between the fourth and fifth ring road in the northwest of Beijing. All the measurements (Massling et al., 2009; Meier et al., 2009; Wu et al., 2016; Wu et al., 2017; Wang et al., 2018c) took place on the roof of a six-floor building (~30 m above ground), which is ~100 m away from a major road.

Aerosol hygroscopic growth was first measured at the PKU site during 2004-2005 (Massling et al., 2009; Meier et al., 2009). Massling et al. (Massling et al., 2009) measured aerosol hygroscopic growth (at 90% RH) in June-July 2004 and January-February 2005. Aerosol

11

Atmospheric
Chemistry
and Physics
Discussions
Open Access
EGU

242 hygroscopicity exhibited trimodal distribution, and κ were found to be in the range of 0-0.028,

243 0.036-0.176 and 0.175-0.386 for the low-, medium- and high-hygroscopic modes (Massling et al.,

244 2009). In addition, no obvious difference in aerosol hygroscopicity was found between summer

245 and winter. Ammonium sulfate was the major inorganic species for the high-hygroscopic mode,

246 while fresh carbonaceous materials (e.g., soot) dominated the low-hygroscopic mode (Massling et

247 al., 2009). Aerosol hygroscopicity was found to increase with particle size and pollution levels

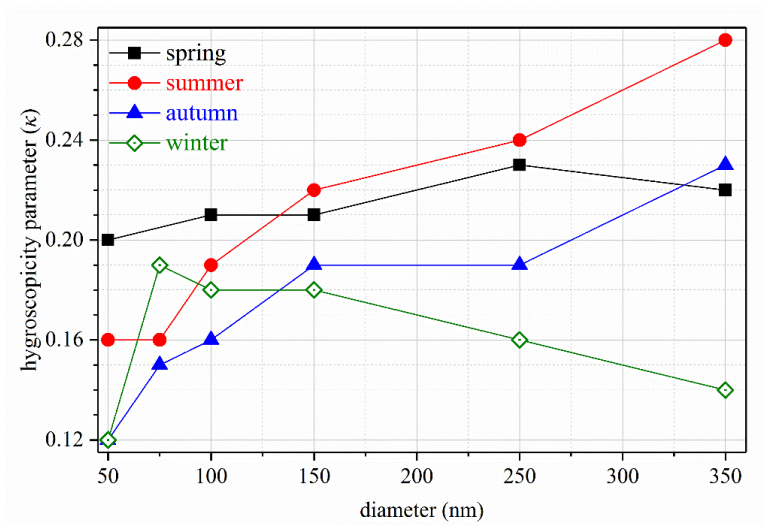248 (Massling et al., 2009), as more secondary inorganic species were formed.

249   Meier et al. (Meier et al., 2009) further explore aerosol hygroscopic growth (at 90% RH) at

250 the PKU site in January 2005. Similar to the work by Massling et al. (Massling et al., 2009), three

251 aerosol hygroscopicity modes were identified, with the κ values being 0-0.027, 0.036-0.154 and

252 0.152-0.366 for low-, medium- and high-hygroscopic modes (Meier et al., 2009); however, no

253 obvious dependence of aerosol hygroscopicity on air pollution levels was found. The average κ

254 were found to first increase (30-80 nm) and then decrease with particle size (80-350 nm). Measured

255 GF at 90% RH were compared with these calculated from size-resolved inorganic compositions

256 measured offline, and discrepancies between measured and calculated GF were attributed to the

257 effects of organics contained (Meier et al., 2009). In addition, hygroscopic growth at 55% and 70%

258 RH was also explored for 30-400 nm aerosol particles (Meier et al., 2009), and GF at 55% and 70%

259 RH, compared to 90% RH, displayed similar dependence on particle size.

260   Wu and co-workers (Wu et al., 2016; Wu et al., 2017; Wang et al., 2018c) carried out

261 exntensive aerosol hygrosocpic growth measurements (at 90% RH) at the PKU site during 2014-

262 2015. Bimodal aerosol hygroscopicity distribution was observed in May-June 2014 (Wu et al.,

263 2016), dominated by the hydrophilic mode, and the average κ appeared to increase with particle

264 size, from 0.160 at 50 nm to 0.280 at 250 nm. In addition, number fractions of aerosol particles in

265   the hydrophilic mode first increased with particle size up to 150 nm, and then did not show

266   significant change with further increase in particle size (Wu et al., 2016); to be more specific,

267   average number fractions of aerosol particles in the hydrophilic mode were ~0.6 at 50 nm and

268   increased to ~0.8 above 150 nm. For each particle size, aerosol hygroscopicity was found to be

269   larger during new particle formation (NPF) periods, compared to non-NPF periods (Wu et al.,

270   2016), because more secondary species were found during NPF periods typically associated with

271   strong photochemical processes. Aerosol mass spectrometry (AMS) measurements suggested that

272   both aerosol hygroscopicity was dominated by inorganics, the contribution of which increased

273   with particle size and pollution levels (Wu et al., 2016). It was further found that the measured κ

274   could be well predicted using the AMS data, and the derived κ of organics depended linearly on

275   their O:C ratios (Wu et al., 2016).

276   The PKU site was affected by a series of biomass burning events in May-June 2014, and the

277   effect of biomass burning on aerosol composition and hygroscopicity was examined (Wu et al.,

278   2017). During biomass burning events, biomass burning contributed significantly to the production

279   and growth of aerosols in the Aitken mode, and the contribution of organics and black carbon to

280   mass concentrations of submicrometer aerosols reached 60% and 18% (Wu et al., 2017).

281   Hygroscopicity and number fractions of aerosols in the hydrophobic mode were relatively

282   invariable during biomass burning events, and the average κ, which showed no variation with

283   particles size (50-250 nm), were determined to be ~0.1 (Wu et al., 2017), substantially smaller than

284   those in the same period without significant impacts by biomass burning (Wu et al., 2016).

Figure 1. Change in average κ with aerosol diameter at the PKU site in four different seasons between May 2014 to January 2015 (Wang et al., 2018c).

Seasonal variation of aerosol hygroscopic growth was investigated at the PKU site from May 2014 to January 2015 (Wang et al., 2018c), and the result is displayed in Figure 1. Average κ increased significantly with particle size (50-350 nm) in summer and autumn, when strong photochemical processes enhanced secondary aerosol formation and led to particle growth (Wang et al., 2018c); in fact, number fractions of particles in the hydrophilic mode increased with pollution levels, and they dominated the accumulation mode when $PM_{2.5}$ mass concentration exceeded 100 $\mu g/m^3$. In contrast, as shown in Figure 1, average κ only increased slightly with particles size (50-350 nm) in spring while decreased substantially with particle size (75-350 nm) in winter (Wang et al., 2018c), indicating significant contribution of primary species to aerosol particles. Furthermore, being different to summer and autumn, substantial amounts of aerosol particles in the hydrophobic mode were always observed in spring and winter (Wang et al., 2018c). Another important feature revealed by Figure 1 is that for 150-350 nm aerosols, the hygroscopicity

301   was always highest in summer and lowest in winter (Wang et al., 2018c), and the difference

302   between the two seasons increased with particle size.

303   In addition, aerosol hygroscopic growth was investigated in March-April 2015 at the roof of

304   the Environmental Science Building (40º0'17''N, 116º19'34''E) on the campus of Tsinghua

305   University (Fajardo et al., 2016). This site, very close to the PKU site, is usually affected by the

306   same air masses. Number size distributions under dry and ambient conditions were measured for

307   10-500 nm particles to explore aerosol hygroscopicity under ambient RH (Fajardo et al., 2016).

308   No obvious aerosol growth was observed for RH below 50% (Fajardo et al., 2016); however, the

309   aerosol volume was increased by ~80% when RH reached 50%, and further increase in ambient

310   RH led to further hygroscopic growth.

311   **IAP site:** The IAP site is located at the Institute of Atmospheric Physics, Chinese Academy

312   of Science (39.97ºN, 116.37ºE) between the third and fourth ring roads in northern Beijing. All the

313   aerosol hygroscopic growth measurements (Wang et al., 2017c; Wang et al., 2019b; Fan et al.,

314   2020; Jin et al., 2020) were conducted at 90% RH at the ground level.

Atmospheric
Chemistry
and Physics
Discussions

315
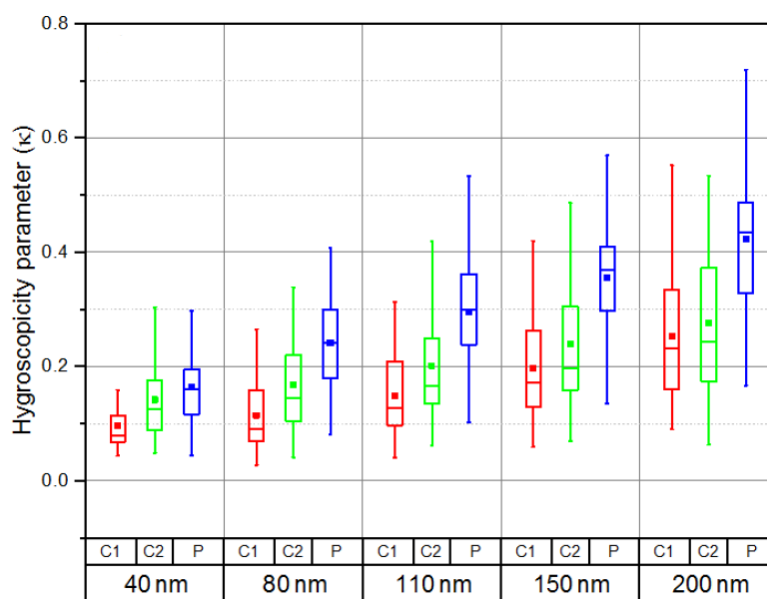
Figure 2. Size-resolved κ during the control clean (C1), the non-control clean (C2) and the non-control polluted (P) periods. Solid squares represent the average κ, boxes represent the 25th, 50th, and 75th percentiles, and extremities represent the 5th and 95th percentiles. Reprint with permission by Wang et al. (Wang et al., 2017c). Copyright 2017 Copernicus Publications.

320

321   Wang et al. (Wang et al., 2017c) investigated aerosol hygroscopic growth at the IAP site in

322   August-October 2015, when emission control measures were implemented for the 2015 China

323   Victory Day parade. Three periods with different pollution levels, including the control clean (C1),

324   the non-control clean (C2) and the non-control polluted (P) periods, were specifically examined to

325   evaluate the effect of emission control. Figure 2 shows that aerosol hygroscopicity increased with

326   particle size and pollution level (Wang et al., 2017c), due to enhanced contribution of secondary

327   species. For example, κ increased from 0.100 at 40 nm to 0.250 at 200 nm during C1, from 0.140

328   at 40 nm to 0.280 at 200 nm during C2, and from 0.160 at 40 nm to 0.420 at 200 nm during the

329   polluted period (Wang et al., 2017c). Furthermore, number fractions of particles in the more

330   hygroscopic mode increased in the polluted period, compared to C1 and C2. For 40 nm particles,

331   a quasi-unimodal hygroscopicity distribution was observed during C1, while bimodal or quasi-

332   trimodal distributions were observed during the other two periods; in contrast, bimodal patterns

333   were always observed for 150 nm particles (Wang et al., 2017c). It was also found that for all the

334   three periods, the average κ were always larger during the daytime than the nighttime (Wang et al.,

335   2017c).

336   A following study (Wang et al., 2019b) measured aerosol hygroscopic growth at the IAP site

337   in November-December 2016. Overall the average κ were found to increase with particle size,

338   from 0.164 at 40 nm to 0.230 at 200 nm during the clean period and from 0.155 at 40 nm to 0.290

339   at 200 nm during the polluted period (Wang et al., 2019b); compared to the clean period, the

340   average κ during the polluted period were smaller for 40 nm particles but larger for 80-200 nm

341   particles. In addition, bimodal distributions were always observed (Wang et al., 2019b). Number

342   fractions of particles in the less-hygroscopic mode was larger for 40 nm particles and smaller for

343   80-200 nm particles during the polluted period (Wang et al., 2019b), when compared to the clean

344   period, reflecting the compositional variation in 40 and 80-200 nm particles during the two periods.

345   Diurnal variation of aerosol hygroscopicity was also explored, displaying significant differences

346   between clean and polluted periods (Wang et al., 2019b).

347   Jin et al. (Jin et al., 2020) further analyzed size-resolved aerosol composition and

348   hygroscopicity measured at the IAP site in November-December 2016 (Wang et al., 2019b). The

349   size-dependent κ derived from measured GF at 90% RH was used to calculate ALWC at ambient

350   RH, assuming that a constant κ could be used to calculate GF at different RH (Jin et al., 2020); in

351   addition, size-resolved aerosol composition measured using AMS was used as input in

352   ISORROPIA-II to simulate ALWC at ambient RH. ALWC simulated using ISORROPIA-II were

353   found to be significantly smaller than calculated ALWC when RH was <60% (Jin et al., 2020),

354   because ISORROPIA-II failed to estimate water uptake by organics at low RH. Overall, organic

355   materials were estimated to contribute to (30±22)% of ALWC (Jin et al., 2020), highlighting the

356   importance of organics to aerosol hygroscopicity in urban Beijing.

357   Fan et al. (Fan et al., 2020) further conducted aerosol hygroscopic growth measurements at

358   the IAP site in May-June 2017, and bimodal hygroscopicity distributions were also observed for

359   40-200 nm aerosols. The summertime measurement in 2017 was compared with the wintertime

360   measurement at the same site in 2016 (Wang et al., 2019b), and the size dependence of aerosol

361   hygroscopicity was found to differ for the two seasons (Fan et al., 2020). The average κ increased

362   from 0.158 at 40 nm to 0.271 at 110 nm in winter, and further increase in particle size (to 200 nm)

363   led to slight decrease in κ (Fan et al., 2020); for comparison, the average κ increased with particles

364   size in summer, from 0.211 at 40 nm to 0.267 at 200 nm (Wang et al., 2019b). It was suggested

365   that the size dependence of aerosol hygroscopicity was mainly determined by the size-resolved

366   mass fractions of secondary inorganic species (Fan et al., 2020).

367   **CAMS site:** Wang et al. (Wang et al., 2018a) measured aerosol hygroscopic growth (30-90%

368   RH) of ambient aerosols on the campus of Chinese Academy of Meteorological Sciences, located

369   between the second and third ring roads in west Beijing. Measurements were conducted on a

370   building roof (~53 m above ground level) in December 2016, and the distance between the site

371   and a major road with heavy traffic was <200 m. Aerosol hygroscopic growth displayed unimodal

372   when RH did not exceed 60%, while bimodal distributions were usually observed at 70% and 80%

373   RH; in addition, aerosol hygroscopic growth occasionally exhibited trimodal distribution at 85%

374   and 90% RH (Wang et al., 2018a). Measured GF at 90% RH were used to calculate κ, which were

Atmospheric
Chemistry
and Physics
Discussions

Open Access

EGU

375   determined to be 0.010-0.015 and 0.286-0.358 for the hydrophobic and hydrophilic modes (Wang

376   et al., 2018a), both increasing with particle size (50-200 nm). Number fractions of hydrophobic

377   particles exceeded 50% at 50 and 100 nm, while hydrophilic particles frequently became dominant

378   in terms of number concentrations at 150 and 200 nm (Wang et al., 2018a). In addition,

379   hygroscopicity decreased at 50 nm but increased at 200 nm during heavily polluted periods (Wang

380   et al., 2018a), indicating their difference in compositions and sources.

381   **3.1.2   Rural sites in Beijing**

382   Aerosol hygroscopic growth were measured at two rural sites in Beijing, including Yufa

383   (Achtert et al., 2009) and Huairou (Wang et al., 2020b). The Yufa site (39.51ºN, 116.31ºE) is ~1.2

384   km away from a high-traffic expressway and ~50 km south to urban Beijing, and can be considered

385   as a representative rural and regional background site. Achtert et al. (Achtert et al., 2009) measured

386   aerosol hygroscopic growth as a function of RH (56, 76, 85 and 91%) on a four-floor building (22

387   m above the ground) at this site in August-September 2006. GF at 91% RH, ranging from 1.15 to

388   1.80 for 30-300 nm particles, were found to be larger in the accumulation mode than the Aitken

389   mode (Achtert et al., 2009); furthermore, increase in mass fractions of sulfate during polluted

390   periods led to increase in aerosol hygroscopicity with pollution level. Diurnal variation of aerosol

391   hygroscopicity was also explored (Achtert et al., 2009): hygroscopicity was found to be higher in

392   the daytime than the nighttime for the Aitken mode, whereas no significant difference in

393   hygroscopicity was observed between daytime and nighttime for the accumulation mode.

394   The Huairou site (40.42ºN, 116.69ºE) is located on the campus of the University of the

395   Chinese Academy of Sciences, ~60 km northeast from the center of Beijing. It was mainly

396   influenced by regional transport of pollutants from downtown Beijing (Tan et al., 2018) and small

397   local sources nearly (e.g., moderate traffic and small residential areas). Aerosol hygroscopic

398   growth (at 90% RH) was measured at this site in January-March 2016 (Wang et al., 2020b). The

399   average κ were determined to be 0.162-0.208 for 50-300 nm particles (Wang et al., 2020b), and

400   mass fractions of nitrate, which contributed significantly to aerosol hygroscopic growth, reached

401   44% during polluted episodes.

402   **3.1.3   Other urban/suburban sites**

403   Aerosol hygroscopic growth was measured at other four urban/suburban sites in NCP,

404   including two sites in Tianjin, one site in Hebei Province and one site in Shanxi Province.

405   **Tianjin:** The Wuqing site is located next to the Wuqing Meteorological Station (39º23'N,

406   117º0'E) in the west area of Wuqing (Tianjin), surrounded by mixed agricultural, residential and

407   industrial regions. This site is a good place to study regional air pollution in NCP, as it is ~30 km

408   northwest to the urban Tianjin, ~80 km southeast to the urban Beijing, ~130 km southwest to

409   Tangshan (Hebei), and ~160 km northeast to Baoding (Hebei). Aerosol hygroscopic growth was

410   measured at three RH (90%, 95% and 98.5%) at this site in July-August 2009 (Liu et al., 2011).

411   Bimodal hygroscopicity distribution was observed over the whole period, and the average κ,

412   derived from GF measured at 90% RH, increased from 0.250 at 50 nm to 0.340 at 250 nm (Liu et

413   al., 2011). Compared to the nighttime, both the average κ and number fractions of particles in the

414   more-hygroscopic mode were larger during the daytime (Liu et al., 2011). The average κ were

415   found to increase with particle size for the more-hygroscopic mode, from 0.310 at 50 nm to 0.390

416   at 250 nm (Liu et al., 2011); in contrast, they decreased with particle size for the nearly

417   hydrophobic mode, from 0.054 at 50 nm to 0.025 at 250 nm. It was found that inorganics play an

418   important role for hygroscopic growth of the accumulation mode (Liu et al., 2014), while organics

419   were very importance for hygroscopic properties of the Aitken mode. In addition, κ calculated

420   from aerosol compositions measured offline were consistent with those derived from H-TDMA

421   measurements (Liu et al., 2014).

422   Two different methods were used to estimate ALWC at the Wuqing site in July-August 2009

423   (Bian et al., 2014). For the first method, κ derived from GF measurements at 90-98.5% RH were

424   assumed to be constant at different RH, and thus ALWC could be calculated from particle number

425   size distribution (Bian et al., 2014); for the second method, size-resolved aerosol composition,

426   only taking into account water soluble inorganic ions, was used as input in ISORROPIA-II to

427   predict ALWC. ALWC estimated using the first method agreed with those using the second method

428   for >60% RH, but was much larger compared to the second method when ambient RH was <60%

429   (Bian et al., 2014).

430   In March 2018, Ding et al. (Ding et al., 2019) carried out aerosol hygroscopic growth

431   measurements (70-85% RH) at the NKU site, an air quality research supersite at Nankai University

432   (38º59'N, 117º20'E), which was ~20 km away from downtown Tianjin. GF measured at 85% RH

433   were used to calculate average κ, being 0.301-0.477, 0.203-0.386 and 0.281-0.419 on 13th, 14th

434   and 15th March (Ding et al., 2019). In addition, the average κ were found to be larger during

435   polluted periods than clean periods, as the contribution of nitrate, sulfate and ammonium in the

436   accumulation mode increased during polluted periods (Ding et al., 2019). It was also found that

437   for the accumulation mode, κ were larger in the nighttime than the daytime (Ding et al., 2019).

438   Water-soluble inorganic ions measured offline were used as input in the ISORROPIA-II to predict

439   aerosol hygroscopicity, and measured and predicted κ showed good agreement (Ding et al., 2019),

440   implying that the contribution of organics to aerosol hygroscopic growth was quite limited.

441   **Hebei Province:** The Xingtai site is located at the National Meteorological Basic Station in

442   Xingtai (37.18ºN, 114.37ºE), a heavily polluted city in the center of NCP, and aerosol hygroscopic

21

443   growth (at 85% RH) was measured at this site in May-June 2016 (Wang et al., 2018b). As shown

444   in Figure 3, quasi-unimodal aerosol hygroscopicity distribution was observed and number

445   fractions of particles in the more-hygroscopic mode was ~90% for 40-200 nm particles (Wang et

446   al., 2018b), indicating that they were highly aged and internally mixed. The average κ were

447   determined to be 0.364-0.39 (Wang et al., 2018b), significantly larger than those reported for most

448   of other sites in NCP. No obvious dependence of average κ on particle size was observed, and the

449   average κ were found to be larger in daytime than nighttime, especially during new particle

450   formation events.

451
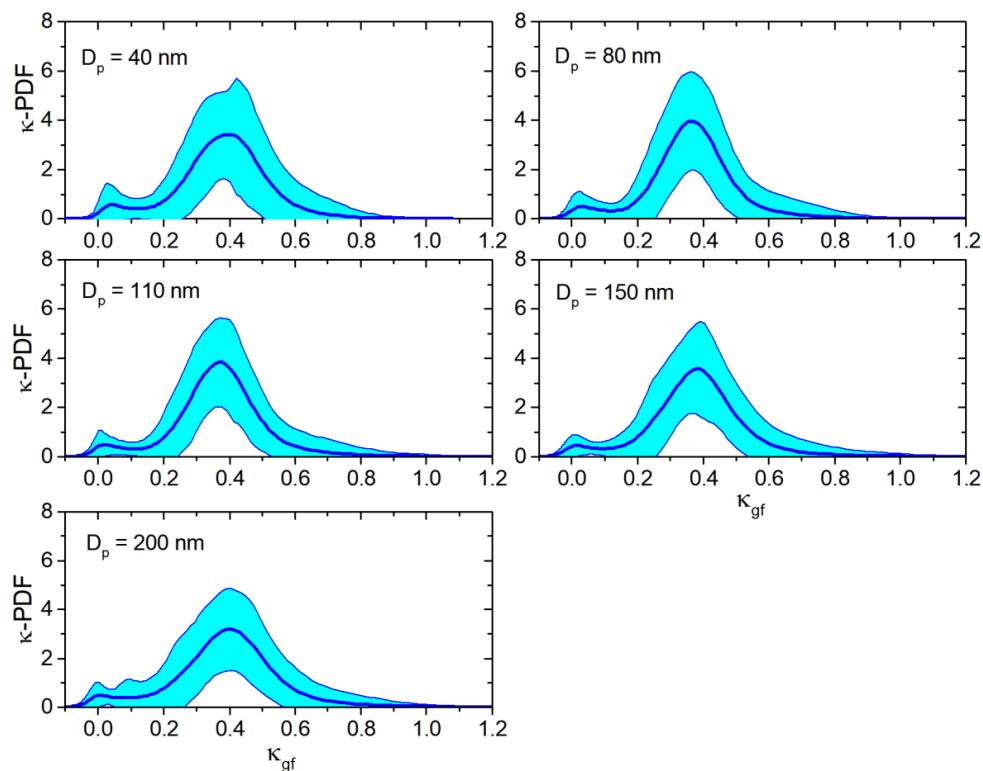
Figure 3. Mean probability density functions of κ and their standard deviations (shaded areas) for

453   40, 80, 110, 150 and 200 nm particles at the Xingtai site in May-June 2016, as derived from

454   measured GF at 85% RH. Reprint with permission by Wang et al. (Wang et al., 2018b). Copyright

455   2018 Copernicus Publication.

456

457   For the campaign at the Xingtai site in May-June 2016 (Wang et al., 2018b), aerosol

458   hygroscopicity on a clean day (21 May) was compared with that on a highly polluted day (23 May).

459   Aerosol hygroscopicity was higher on the polluted day (Chen et al., 2019), likely due to the

460   enhanced formation of nitrate as revealed by ACSM (aerosol chemical speciation monitor)

461   measurements. Furthermore, aerosol hygroscopicity increased with particles size (40-200 nm) on

462   both days, from 0.288 to 0.339 on 21 May and from 0.325-0.352 on 23 May (Chen et al., 2019).

463   **Shanxi Province:** The Xinzhou site (38.24ºN, 112.43ºE, 1500 m above sea level) was located

464   on the border between the NCP and the Loess Plateau. This suburban and regional site, surrounded

465   by agricultural land with limited local anthropogenic emissions, was located ~360 km southwest

466   to Beijing, ~78 km northwest to Taiyuan and ~10 km south to the city nearby. Aerosol hygroscopic

467   growth (85% RH) was investigated for 25-200 nm aerosols at this site in July-August 2014 (Zhang

468   et al., 2017). Quasi-unimodal aerosol hygroscopicity distribution was observed, indicating highly

469   aged and internally mixed particles. The average κ were determined to be 0.420-0.528,

470   significantly larger than those observed at other sites in the NCP; in addition, no obvious

471   dependence of κ on particle size was found (Zhang et al., 2017).

472   **3.1.4   Other rural sites**

473   Aerosol hygroscopic growth was measured at other two rural sites in NCP, i.e. the Xianghe

474   site and the Wangdu site (both in Hebei). The Xianghe site (39.75ºN, 116.96ºE), surrounded by

475   residential areas and farmlands, is considered as a typical rural site in NCP and is located ~5 km

476   west to the center of Xianghe town and ~70 km southeast to Beijing. At this site, aerosol

477   hygroscopic growth (at 87% RH) was measured in July-August 2013 (Zhang et al., 2016b).

478   Trimodal aerosol hygroscopicity distributions were observed for 50-350 nm particles (Zhang et al.,

479   2016b), and the average κ were determined to be 0.020-0.056, 0.170-0.211 and 0.365-0.455 for

480   nearly-hydrophobic, less-hygroscopic and more-hygroscopic modes. Aerosol hygroscopicity

481   showed some dependence on air masses (Zhang et al., 2016b): air masses which were transported

482   from the north with high speed winds typically contained larger number fractions of hydrophobic

483   species and exhibited lower hygroscopicity, whereas no obvious difference in aerosol

484   hygroscopicity and mixing state were observed for other air masses.

485   The Wangdu site (38.71ºN, 115.16ºE), a rural site located in the center area of NCP, was ~200

486   km southwest to Beijing, and aerosol hygroscopic growth (at 90% RH) was measured at this site

487   in June 2014 (Wang et al., 2017b). Bimodal aerosol hygroscopicity distribution was always

488   observed (Wang et al., 2017b), and the average κ were found to increase with particle size, from

489   0.240 at 30 nm to 0.320 at 250 nm.

490   **3.2 Yangtze River Delta (YRD)**

491   A number of aerosol hygroscopic growth measurements have been carried out since 2009 in

492   three large cities (Shanghai, Hangzhou and Nanjing) in the Yangtze River Delta.

493   **3.2.1   Shanghai**

494   Ambient aerosol hygroscopic growth was measured at two sites in Shanghai (Ye et al., 2011;

495   Ye et al., 2013; Wang et al., 2014; Xie et al., 2017; Li et al., 2018; Wang et al., 2020a). The FDU

496   site (31°18'N, 121°29'E) is located on the building roof of Department of Environmental Science

497   and Engineering, Fudan University; the Pudong site (31.22ºN, 121.55ºE) is located in Pudong

498   Meteorological Bureau. Both sites are considered as urban sites, surrounded by residential,

499   industrial and traffic areas, and their distance is <10 km.

500   **FDU site:** At the FDU site, Ye et al. (Ye et al., 2011) measured aerosol hygroscopic growth

501   (30-200 nm) at 20-85% RH in January-February 2009. Bimodal hygroscopic growth distribution

502   was always observed at 85% RH, and κ derived from measured GF at 85% RH were determined

503   to be 0.027-0.063 and 0.291-0.381 for the less- and more-hygroscopic modes (Ye et al., 2011). The

504   average κ decreased with particle size for the less hygroscopic mode while increased with particle

505   size for the more hygroscopic mode (Ye et al., 2011); in addition, number fractions of particles in

506   the less hygroscopic mode decreased with particle size. The change in GF with RH (20-85%) was

507   also discussed for particles with different sizes (Ye et al., 2011).

508   Compositional data provided by ATOFMS (Aerosol Time-of-Flight Mass Spectrometry) were

509   used to interpret GF measured at 85% RH for 250 nm particles on 18-19 January and 10 February

510   2009 (Ye et al., 2011). Bimodal aerosol hygroscopicity distribution was observed for 250 nm

511   particles, including a nearly-hydrophobic mode with κ of 0.029-0.061 and a more-hygroscopic

512   mode with κ of 0.387-0.399 (Wang et al., 2014). Aerosols in the more-hygroscopic mode consisted

513   predominantly of secondary species (e.g., OC-amine, sulfate and nitrate), while biomass burning

514   aerosols, uncoated EC, secondary organic compounds, and dust/ash were frequently identified in

515   the nearly-hydrophobic mode (Wang et al., 2014).

516   Aerosol hygroscopic growth (at 85% RH) was also measured at this site in February-March

517   2014 (Wang et al., 2020a). Aerosol hygroscopicity was found to exhibit bimodal distribution at

518   250 nm, and the average κ were determined to be 0.029 and 0.376 for nearly-hydrophobic and

519   more-hydrophilic modes (Wang et al., 2020a). Nearly-hydrophobic particles typically included

520   biomass burning aerosol, fresh EC and high molecular mass OC, while more-hydrophilic particles

521   included aged EC, amine-rich particles, and etc. (Wang et al., 2020a). Furthermore, a statistic

Atmospheric
Chemistry
and Physics
Discussions

Open Access

EGU

522   method was developed to estimate aerosol hygroscopicity from single particles mass spectra

523   (Wang et al., 2020a).

524   Xie et al. (Xie et al., 2017) further measured aerosol hygroscopic growth (83% RH) at the FDU

525   site in December 2014-January 2015. Bimodal aerosol hygroscopicity distribution (nearly

526   hydrophobic and more hygroscopic modes) was usually observed, and the average κ increased

527   from 0.161 at 40 nm to 0.345 at 400 nm (Xie et al., 2017). Number fractions of nearly hydrophobic

528   particles increased during polluted periods for all the sizes considered (40-400 nm), indicating

529   significant contribution of primary particles during haze events (Xie et al., 2017); however, the

530   increase in number fractions of nearly hydrophobic particles during pollution events were less

531   significant for larger particles, suggesting that primary emissions contributed more to smaller

532   particles.

533   Mixing state and hygroscopic growth (at 85% RH) were explored at the FDU site in July 2017

534   specifically for ambient black carbon (BC) aerosols (120, 240 and 260 nm) (Li et al., 2018).

535   Number fractions of BC particles decreased with particle size, from ~80% for 120 nm to ~60% for

536   360 nm. Hygroscopicity of BC particles displayed unimodal distribution, and their GF at 85% RH

537   peaked at ~1.0 (Li et al., 2018). Enhancement in hygroscopicity of BC particles, due to their aging

538   via condensation of secondary species, was frequently observed (Li et al., 2018): during the

539   nighttime nitrate contributed significantly to BC aging, while formation of secondary organic

540   materials played an important role during the daytime.

541   **Pudong site:** Aerosol hygroscopic growth (at 91% RH) was studied at the Pudong site in

542   September 2009 (Ye et al., 2013). As shown in Figure 4, aerosol hygroscopicity was found to be

543   trimodal, including a nearly-hydrophobic mode and a more-hygroscopic mode, as well as a less-

544   hygroscopic mode with much less abundance (Ye et al., 2013). The average κ increased from 0.270

545   at 30 nm to 0.390 at 200 nm for the more-hygroscopic mode (Ye et al., 2013), and decreased from

546   0.054 at 30 nm to 0.011 at 200 nm for the nearly-hydrophobic mode.

547
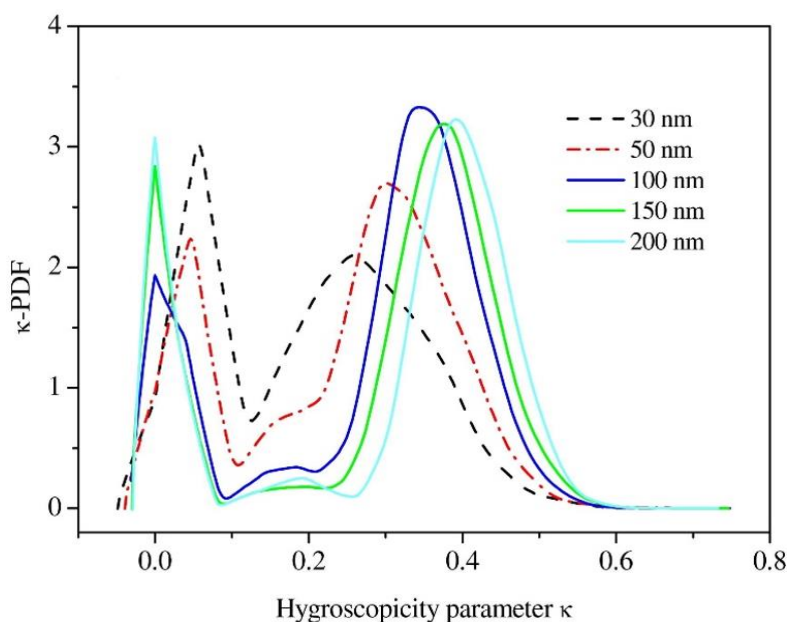
Figure 4. Probability distribution functions of the hygroscopicity parameter (κ) for 30, 50, 100,

549   150 and 200 nm aerosols at the Pudong site in September 2009. Reprint with permission by Ye et

550   al. (Ye et al., 2013). Copyright 2013 Elsevier Ltd.

551

3.2.2   Hangzhou

553   Up to now only one aerosol hygroscopic growth study was carried out in Hangzhou, at the ZJU

554   site located on the Huajiachi campus of Zhejiang University (30°16'N, 120°11'E). Aerosol

555   hygroscopic growth was measured at 70-90% RH (mainly at 82%) in December 2009-January

556   2010 (Zhang et al., 2011). Bimodal hygroscopicity distribution was observed for 50-200 nm

557   aerosols, while unimodal hygroscopicity distribution was observed for 30 nm aerosols (Zhang et

558   al., 2011). The average κ decreased from 0.121 at 30 nm to 0.065 at 80 nm for the low-hygroscopic

559   mode, and further increase in particle size (up to 200 nm) did not lead to significant change in κ

560   (Zhang et al., 2011). For comparison, the average κ increased from 0.303 at 30 nm to 0.343 at 80

561   nm for the more-hygroscopicity mode, and further increase in particle size only resulted in very

562   small increase in κ. In addition, number fractions of particles in the more-hygroscopic mode

563   increased from ~48% at 30 nm to ~70% at 100 nm, and remained nearly constant for 100-200 nm

564   (Zhang et al., 2011).

565   **3.2.3   Nanjing**

566   Aerosol hygroscopic growth was measured at three urban/suburban sites in Nanjing. The

567   NUIST site (32°207'N, 118°717'E) is a suburban site located on the 12th floor of the Meteorological

568   building at Nanjing University of Information Science and Technology, with several large

569   petrochemical factories and a busy expressway nearby. The NATC site (32.0°N, 118.7°E) is a

570   typical urban site at Nanjing Advanced Technical College, located in the centre business district

571   with heavy residential and traffic emissions. The JEMC site is an urban site on the 6th floor of the

572   building of Jiangsu Environmental Monitoring Centre (~18 m above the ground), located in the

573   urban area and surrounded by a variety of sources such as residence, restaurants, office blocks and

574   traffic.

575   **NUIST site:** Wu et al. (Wu et al., 2014) measured aerosol hygroscopic growth as a function of

576   RH (60-90%) at the NUIST site in May-July 2012, and bimodal hygroscopicity distributions were

577   frequently observed at 90% RH for 40-200 nm aerosols. For the more-hygroscopic mode, κ were

578   determined to be 0.294-0.349, increasing with particle size (except for 40 nm); while for the less-

579   hygroscopic mode, κ were found to decrease with particle size, from 0.079 at 40 nm to 0.040 at

580   200 nm (Wu et al., 2014). The average aerosol hygroscopicity measured at this site in Nanjing

581   seemed to be slightly lower than those reported in Beijing, Shanghai and Guangzhou.

582 Yang and co-workers further investigated aerosol (30-230 nm) hygroscopic growth (at 90%

583 RH) at this site in April-May 2014 (Xu et al., 2015; Yang et al., 2019), and bimodal hygroscopicity

584 distribution was observed. The κ values were found to be very low (close to 0) for the low-

585 hygroscopic mode, and decreased from 0.232 at 30 nm to 0.186 at 230 nm for the medium

586 hygroscopic mode. Aerosol hygroscopicity measured in April-May 2014 (Xu et al., 2015; Yang et

587 al., 2019) were significantly lower than that measured in May-June 2012 at the same site (Wu et

588 al., 2014). One possible reason was that in April-May 2014 organic species made a large

589 contribution to submicrometer aerosols (21-38% by mass) (Xu et al., 2015; Yang et al., 2019), thus

590 leading to substantial decrease in aerosol hygroscopicity.

591 **NATC site:** In August 2013, Li et al. (Li et al., 2015b) investigated hygroscopic growth at 90%

592 RH for 32-350 nm aerosols. A less-hydrophobic mode (κ: 0.017-0.031) and a more-hygroscopic

593 mode (κ: 0.178-0.229) were observed during the campaign (Li et al., 2015b). Aerosol

594 hygroscopicity reported at the NATC site in August 2013 (Li et al., 2015b) was lower than these

595 reported at the NUIST site in May-June 2012 (Wu et al., 2014) and in April-May 2014 (Xu et al.,

596 2015; Yang et al., 2019), perhaps because the contribution of low hygroscopic primary particles

597 (e.g., soot) from local emission was larger at the NATC site (an urban site), compared to the

598 NUIST site (a suburban site).

599 **JEMC site:** At the JEMS site, 40-200 nm aerosol hygroscopic growth was measured at 85%

600 RH in January-February 2015 (Zhang et al., 2018). The average κ were determined to be 0.200-

601 0.271 for 40-200 nm particles (Zhang et al., 2018), significantly larger than those (0.081-0.126 for

602 32-350 nm particles) reported for the NATC site in August 2013 (Li et al., 2015b), and the reason

603 was unclear. Bimodal hygroscopicity distribution was also observed (Zhang et al., 2018); similar

604 to two previous studies in Nanjing (Wu et al., 2014; Li et al., 2015b), number fractions of particles

605 in the low hygroscopic mode and their average κ both decreased with particle size, while the

606 average κ increased with particle size for the more hygroscopic mode (except for 40 nm).

607 3.3 Pearl River Delta (PRD)

608   A series of aerosol hygroscopic growth studies were conducted in PRD, to be more specific, at

609 two rural sites (Xinken and Wanqinsha) and one suburban site (Panyu) in Guangzhou and one

610 suburban site (HKUST) in Hong Kong.

611 3.3.1   Rural sites in Guangzhou

612   The Xinken site (22.6°N, 113.6°E), located near the Pearl River estuary, is ~50 km southeast

613 to urban Guangzhou, and the Wanqinsha site is located ~9 km northwest of Xinken. Both are

614 typical rural background sites with no major pollution sources nearby, and air quality at both sites

615 are affected by regional transport combined with limited local sources, such as traffic, ships,

616 biomass burning and cooking (Cheng et al., 2006; Eichler et al., 2008; Kim et al., 2011).

617   Eichler et al. (Eichler et al., 2008) measured aerosol hygroscopic growth (30-91% RH) at the

618 Xinken site in October-November 2004. The average GF at 91% RH were determined to 1.45,

619 1.53, 1.6 and 1.56 for 80, 140, 250 and 380 nm particles (Eichler et al., 2008), corresponding to κ

620 of 0.244, 0.283, 0.324 and 0.288, respectively. Inorganic aerosol compositions measured offline

621 were used to calculate GF, and the average difference between the measured and calculated GF

622 was found to be <8% (Eichler et al., 2008), suggesting that the contribution of organics to aerosol

623 hygroscopicity was rather small.

624   In a following study (Kim et al., 2011), aerosol hygroscopic growth (at 85% RH) of ultrafine

625 particles (40, 50, 60 and 80 nm) was investigated at the Wanqinsha site in October-November 2008.

626 During photochemical events, GF varied between 1.13 and 1.55, and particles consisted mainly of

627 ammonium sulfate and organic materials (Kim et al., 2011). For comparison, during combustion

628   events (i.e. affected by biomass burning and traffic emission), aerosol particles were mainly

629   composed of non-hygroscopic carbonaceous species and smaller amounts of potassium, and

630   correspondingly measured GF were reduced to 1.05-1.15 (Kim et al., 2011).

631   **3.3.2   Urban/suburban sites in Guangzhou**

632   The Panyu site, located at the top of Mt. Dazhengang (23º00'N, 113º21'E, 150 m above the sea

633   level), is surrounded by residential areas without major pollution sources nearby and can be

634   considered as a suburban site in Guangzhou (Tan et al., 2013). Several aerosol hygroscopic growth

635   measurements at 90% RH have been carried out at this site since 2011 (Tan et al., 2013; Jiang et

636   al., 2016; Cai et al., 2017; Tan et al., 2017; Cai et al., 2018; Hong et al., 2018; Liu et al., 2018).

637   Aerosol hygroscopic growth was first measured at this site in November-December 2011 (Tan

638   et al., 2013). Bimodal hygroscopicity distributions were observed for 40, 80, 110, 150 and 200 nm

639   particles, and κ were determined to be 0.045-0.091 and 0.290-0.323 for the less- and more-

640   hygroscopic modes (Tan et al., 2013). In general, both hygroscopicity and number fractions

641   increased with particle size for the more-hygroscopic mode, whereas they both decreased with

642   particle size for the less-hygroscopic mode. Average hygroscopicity was found to be larger during

643   the daytime than the nighttime for both modes (Tan et al., 2013), and hygroscopicity and number

644   fractions of particles in the more-hygroscopic mode increased during polluted periods, when

645   compared to clean periods.

646   Jiang et al. (Jiang et al., 2016) compared aerosol hygroscopicity measured at this site between

647   winter (December 2012-January 2013) and summer (July-September 2013), and no obvious

648   difference in average κ was found between the two seasons. Trimodal hygroscopicity distributions

649   were observed for 40-200 nm particles, and κ were determined to be 0.290-0.339, ~0.15 and ~0.015

650   for more-, less- and non-hygroscopic modes (Jiang et al., 2016). Similar to the work by Tan et al.

651　(Tan et al., 2013), hygroscopicity and number fractions increased with particle size for the more-

652　hygroscopic mode, with no distinct difference between winter and summer (Jiang et al., 2016); for

653　the non-hygroscopic mode, hygroscopicity and number fractions both decreased with particle size,

654　and their number fractions were slightly lower in winter than in summer. Furthermore, the average

655　κ were larger during daytime than nighttime for both seasons, and the diurnal variation was more

656　profound in summer (Jiang et al., 2016).

657　　　　Tan et al. (Tan et al., 2017) measured aerosol hygroscopic growth in January-March 2014, and

658　κ increased from 0.204 at 40 nm to 0.312 at 200 nm. The κ values derived from GF measured at

659　90% RH were used to calculate ALWC under ambient conditions, and meanwhile aerosol inorganic

660　species measured were used as input in ISORROPIA-II to predict ALWC. Good agreement

661　between calculated and predicted ALWC were found for RH >70%, but significant differences

662　were found at <70% RH (Tan et al., 2017). Liu et al. (Liu et al., 2018) further explored aerosol

663　hygroscopic growth measured in February-March 2014 at this site, and found that he average κ

664　values increased from 0.261 at 80 nm to 0.323 at 200 nm. In addition, bimodal hygroscopicity

665　distribution was observed, and κ increased from 0.382 at 80 nm to 0.432 at 200 nm for the more

666　hygroscopic mode (Liu et al., 2018).

667　　　　Aerosol hygroscopic growth (at 90% RH) were further measured at this site in November-

668　December 2014 (Cai et al., 2017; Cai et al., 2018). Bimodal hygroscopicity distributions were

669　observed for 40-200 nm particles, and the average κ increased with particle size, from 0.213 at 40

670　nm to 0.312 at 200 nm. The κ values derived from size-resolved chemical compositions measured

671　using AMS were significantly lower than those derived from GF measurements (Cai et al., 2017;

672　Cai et al., 2018), probably because using a constant κ value (0.1) may underestimate

673　hygroscopicity of aerosol organics.

674 Aerosol composition and hygroscopic growth at 90% RH were investigated at this site in

675 September-October 2016 (Hong et al., 2018), using an ACSM and a H-TDMA. Bimodal

676 hygroscopicity distributions were observed; the more-hygroscopic mode was dominant at 100 and

677 145 nm, while less- and more-hygroscopic modes were of similar magnitude at 30 and 60 nm

678 (Hong et al., 2018). The average aerosol hygroscopicity increased with particle size, and no

679 obvious diurnal variation was observed (Hong et al., 2018); however, aerosol hygroscopicity was

680 higher during the daytime for the less-hygroscopic mode while slightly lower in the afternoon for

681 the more-hygroscopic mode. Hygroscopicity closure analysis suggested that taking into account

682 the dependence of GF on composition for organics led to better agreement between measured and

683 calculated GF (Hong et al., 2018). It was further found that GF increased linearly with O:C ratios

684 for organics, and the derived GF appeared to be less sensitive to the changes of O:C ratios during

685 polluted periods.

686 **3.3.3   Hong Kong**

687 Since 2011, H-TDMA and online mass spectrometry were employed by Chan and co-workers

688 (Lopez-Yglesias et al., 2014; Yeung et al., 2014; Cheung et al., 2015) to investigate aerosol

689 composition and hygroscopic growth at the HKUST supersite (22º20'N, 114º16'E) on the east coast

690 of Hong Kong. It is a typical suburban and coastal site with no major pollution sources nearby.

691 Aerosol hygroscopic growth at 90% RH was first investigated at this site in 2011 (Yeung et al.,

692 2014), and bimodal aerosol hygroscopicity distributions were observed with a dominant more-

693 hygroscopic mode and a weak less-hygroscopic mode at 75, 100, 150 and 200 nm. The average κ

694 were determined to be 0.330-0.360 during May, 0.370-0.390 during the first half of September,

695 0.210-0.250 during the second half of September and 0.290-0.320 during November (Yeung et al.,

696   2014), caused by compositional variations in different air masses; however, no obvious

697   dependence of average κ on particle size was found.

698   Number fractions of particles in the more-hygroscopic mode were always >0.8 (Yeung et al.,

699   2014), except for 75 nm particles in the second half of September (~0.45) which was dominantly

700   affected by continental air masses. When compared to maritime aerosols, hygroscopicity of

701   aerosols in the more-hygroscopic mode was substantially lower for continental aerosols which

702   contained larger proportions of organic materials (Yeung et al., 2014). Hygroscopicity closure

703   analysis suggested that using a constant GF (1.18) at 90% RH for organic materials, instead of

704   considering the dependence of GF on their oxidation degree, would lead to better agreement

705   between measured and calculated GF (Yeung et al., 2014), likely because inorganic species (such

706   as sulfate) contributed dominantly to the overall aerosol hygroscopicity during the entire campaign.

707   In addition, hygroscopic growth at the HKUST site was investigated as a function of RH (10-

708   90%) in 2011-2012 (Lopez-Yglesias et al., 2014; Cheung et al., 2015), and both hysteresis behavior

709   and continuous hygroscopic growth of ambient aerosols were observed.

3.4 Other locations

711   In addition to NCP, YRD and PRD, measurements of aerosol hygroscopic growth were also

712   conducted in other regions in China, as discussed below.

713   **Taipei:** Hygroscopic growth (15-90% RH) was investigated for 53, 82, 95 and 202 nm aerosols

714   at an urban site in Taipei (Taiwan Province) in October-December 2001 (Chen et al., 2003).

715   Bimodal hygroscopicity distribution was observed for all the particles at 90% RH: while κ (0.049-

716   0.068) showed no obvious dependence on particle size for the less hygroscopic mode, they

717   increased from 0.274 at 53 nm to 0.422 at 202 nm for the more hygroscopic mode (Chen et al.,

718   2003). No obvious hygroscopic growth was observed at <45% RH (Chen et al., 2003), and bimodal

719   hygroscopic growth behavior appeared at ~76% RH for all the sizes (53-202 nm), becoming more

720   noticeable with further increase in RH.

721   **Mt. Huang:** Mt. Huang (30º08'N, 118º09'E) is located in the mountainous area of east China

722   with large forest coverages and limited anthropogenic activities. Aerosol hygroscopic growth at

723   50-85% RH was examined in September-October 2012 at the mountain foot (~464 m above the

724   sea level) and the mountain top (~1860 m above the sea level) (Wu et al., 2018a). No significant

725   particle growth was observed below 60% RH at both sites, and bimodal growth behavior appeared

726   at ~75% RH except 40 nm particles and became more evident at higher RH (Wu et al., 2018a).

727   Hygroscopicity was higher in the daytime than the nighttime for both modes. In addition,

728   hygroscopicity was slightly higher at the mountain foot than the mountain top for both modes

729   (except 200 nm particles in the more-hygroscopic mode) (Wu et al., 2018a); the reason was that

730   more secondary inorganic species were formed at the mountain foot due to human activities, while

731   on the mountain top the contribution of organics increased. Compared to NCP, YRD and PRD sites,

732   the overall aerosol hygroscopicity was lower at Mt. Huang (Wu et al., 2018a), as it is located in a

733   clean region with smaller fractions of secondary inorganic aerosols.

734   In July 2014 aerosol hygroscopic growth (at 85% RH) was further studied at the top of Mt.

735   Huang (Xu, 2015; Chen et al., 2016; Wang et al., 2016). The average κ were determined to be

736   0.275, 0.266 and 0.290 at 70, 150 and 230 nm (Chen et al., 2016; Wang et al., 2016), in good

737   agreement with the previous study conducted at the same site in 2012 (Wu et al., 2018a). At a

738   given particle size, aerosol hygroscopicity was found to be higher in the daytime than the nighttime

739   (Chen et al., 2016; Wang et al., 2016); furthermore, aerosol hygroscopicity was higher for air

740   masses from northwest than those from southeast. The derived κ depended positively on mass

741   fractions of inorganics and negatively on organics (Chen et al., 2016; Wang et al., 2016). In

742   addition, unimodal aerosol hygroscopicity distribution occurred with high frequency (47.5%)

743   during the campaign, and it also appeared more frequently in the afternoon with GF (at 85% RH)

744   in the range of 1.25-1.45 (Chen et al., 2016; Wang et al., 2016).

745   **Shouxian:** In June-July 2016, Qian et al. (Qian et al., 2017) studied hygroscopic growth (at

746   90% RH) of 50-250 nm aerosols at Shouxian National Climate Observatory (32º26'N, 116º48'E)

747   in east China, a rural site surrounded by farmlands at Shouxian, Anhui Province. Bimodal aerosol

748   hygroscopicity distribution was observed, and the average κ increased with particle size, from

749   0.129 at 50 nm to 0.279 at 250 nm (Qian et al., 2017).

750   **East China Sea:** Total suspended particles were collected during a cruise over the East China

751   Sea (22-35ºN and 119-126ºE) in May-June 2014 and dissolved in deionized water. The resulting

752   solutions were atomized to generated aerosols, and their hygroscopic growth was then measured

753   at 5-90% RH (Yan et al., 2017). The average κ was determined to be 0.88 for the whole cruise, and

754   the daytime average (0.81) was smaller than the nighttime average (0.95) (Yan et al., 2017), due

755   to less chloride loss in the nighttime. It is to be assessed to which extent aerosols generated by Yan

756   et al. (Yan et al., 2017) can actually mimic ambient aerosols.

757   **3.5 Summary**

758   Geographically speaking, almost all the aerosol hygroscopic growth studies were conducted in

759   east China, especially in NCP, YRD and PRD. Aerosol hygroscopic growth in other regions in

760   China remains to be explored, and measurements at rural and remote areas with limited

761   anthropogenic impacts are very scarce. In addition, previous measurements were mainly

762   performed at or close to the ground level, except these carried out on the top of Mt. Huang (Chen

763   et al., 2016; Wang et al., 2016; Wu et al., 2018a).

764   It can be concluded that submicrometer aerosols in China usually exhibit bimodal

765   hygroscopicity distribution (i.e. nearly-hydrophobic and more-hygroscopic modes). However,

766   trimodal distributions, with a medium-hygroscopic mode with limited importance, were also

767   reported by several studies (Massling et al., 2009; Meier et al., 2009; Ye et al., 2013; Jiang et al.,

768   2016; Zhang et al., 2016b; Wang et al., 2017c; Wang et al., 2018a), and quasi-unimodal

769   hygroscopicity distributions existed but were quite sparse (Chen et al., 2016; Wang et al., 2016;

770   Wang et al., 2017c; Zhang et al., 2017; Wang et al., 2018b).

771   For the more-hygroscopic mode, κ usually increased with particle size, except for the

772   measurements carried out at HKUST site (Yeung et al., 2014) where no obvious dependence on

773   particle diameter was found. For the nearly-hydrophobic mode, κ usually decreased with particle

774   size (Liu et al., 2011; Ye et al., 2011; Zhang et al., 2011; Tan et al., 2013; Ye et al., 2013; Wu et al.,

775   2014; Jiang et al., 2016; Zhang et al., 2016b; Qian et al., 2017; Zhang et al., 2018), though different

776   results were also reported in several studies (Chen et al., 2003; Massling et al., 2009; Meier et al.,

777   2009; Li et al., 2015b; Wang et al., 2018a; Wu et al., 2018a).

778   Average aerosol hygroscopicity, especially for the more-hygroscopic mode, usually increased

779   with pollution levels (Massling et al., 2009; Wu et al., 2016; Wang et al., 2017c; Wang et al., 2018a;

780   Chen et al., 2019; Ding et al., 2019; Wang et al., 2019b), attributed to increased mass fractions of

781   secondary inorganic aerosols. However, different results were also reported (Meier et al., 2009),

782   especially for particles at or below 50 nm (Achtert et al., 2009; Wang et al., 2018a; Wang et al.,

783   2019b) for which primary emissions could play an important role.

784   A few studies examined aerosol hygroscopic growth at different seasons (Massling et al., 2009;

785   Jiang et al., 2016; Wang et al., 2018c; Fan et al., 2020). No obvious difference in the overall aerosol

786   hygroscopicity was observed between summer and winter at the PKU site (Beijing) (Massling et

787   al., 2009), the IAP site (Beijing) (Fan et al., 2020) and the Panyu site (Guangzhou) (Jiang et al.,

788   2016). However, one study (Wang et al., 2018c) suggested that the overall hygroscopicity, and

789   especially hygroscopicity of 150-350 particles, was highest in summer and lowest in winter at the

790   PKU site (Beijing).

791   Diurnal variations of aerosol hygroscopic growth were also investigated. Most of these studies

792   suggested that aerosol hygroscopicity was generally higher in the daytime, compared to the

793   nighttime. For example, hygroscopicity was higher in the daytime than the nighttime for the Aitken

794   mode at the Yufa site (Beijing) in August-September 2006 (Achtert et al., 2009), while no

795   significant difference was found between daytime and nighttime for the accumulation mode. In

796   addition, aerosol hygroscopicity was found to be higher at the daytime than the nighttime at the

797   IAP site (Beijing) in August-October 2015 (Wang et al., 2017c), at the Wuqing site (Tianjin) in

798   July-August 2009 for the more hygroscopic mode (Liu et al., 2011), at the Xingtai site (Hebei) in

799   May-June 2016 (Wang et al., 2018b), at the Panyu site (Guangzhou) in November-December 2011

800   (Tan et al., 2013), December 2012-Janurary 2013 (Jiang et al., 2016) and July-September 2013

801   (Jiang et al., 2016), and at Mt. Huang in September-October 2012 (Wu et al., 2018a) and July 2014

802   (Chen et al., 2016; Wang et al., 2016). The underlying reason might be that photochemical

803   processes led to increased relative contribution of secondary aerosols. However, there are also

804   expectations. For example, κ was larger in the nighttime than the daytime for the accumulation

805   mode at the NKU site (Tianjin) in March 2017 (Ding et al., 2019). In addition, no obvious diurnal

806   variation in average aerosol hygroscopicity was observed at the Panyu site (Guangzhou) in

807   September-October 2016 (Hong et al., 2018), though aerosol hygroscopicity was higher during the

808   daytime for the less hygroscopic mode and slightly lower in the afternoon for the more-

809   hygroscopic mode.

810   While aerosol hygroscopic growth measurements were typically carried out at a single RH at

811   around 90%, several studies also investigated aerosol hygroscopic growth as different RH (Chen

812   et al., 2003; Eichler et al., 2008; Achtert et al., 2009; Meier et al., 2009; Liu et al., 2011; Ye et al.,

813   2011; Zhang et al., 2011; Cheung et al., 2015; Wang et al., 2018a; Wu et al., 2018a). As shown in

814   Figure 5, for the measurement carried out at ZJU site (Hangzhou) in December 2009-January 2010

815   (Zhang et al., 2011), κ derived from measured GF at different RH (73-88%) varied from 0.186 to

816   0.244 for 150 nm particles and from 0.184 to 0.252 for 200 nm particles. For the measurement

817   carried out at the Yufa site (Beijing) in August-September 2006 (Achtert et al., 2009), κ were found

818   to decrease with increasing RH (56-91%) for 250 nm particles, varying from ~0.3 to ~0.8.

819   Considerable variations of κ with RH were also reported in other studies (Chen et al., 2003; Meier

820   et al., 2009; Ye et al., 2011; Cheung et al., 2015). Therefore, it can be concluded that using a

821   constant κ to describe aerosol hygroscopic growth at different RH may not always be proper. In

822   addition, during most H-TDMA measurements aerosols were first dried at low RH (typically <15%)

823   and then humidified to a given RH, and as a result these measurements could not simulate the

824   formation of supersaturated droplets which may exist even when RH was below the corresponding

825   deliquescence RH but above the efflorescence RH.
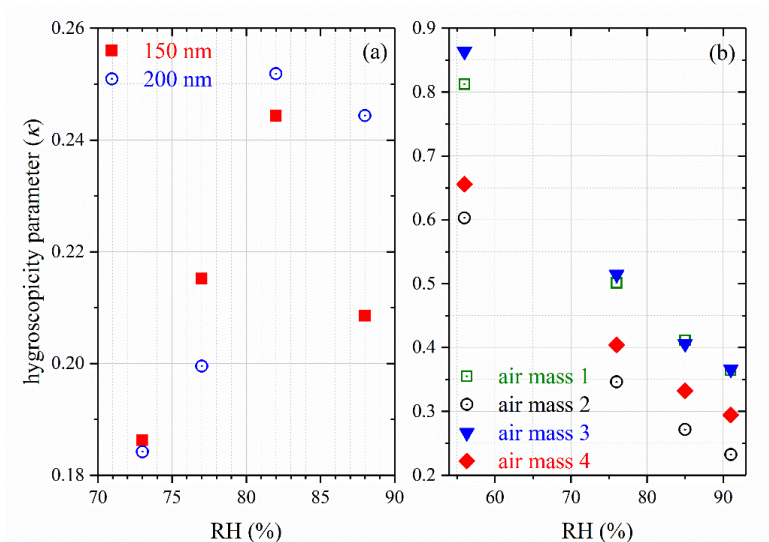
Figure 5. Single hygroscopicity parameters (κ) derived from GF measured as different RH. (a) 150 and 200 nm particles at the ZJU site (Hangzhou) in December 2009-January 2010 (Zhang et al., 2011); (b) 250 nm particles at the Yufa site (Beijing) in August-September 2006 for four typical air masses (Achtert et al., 2009).

4 CCN activities

As stated in Section 2.2, we only discuss CCN activity measurements which reported κ values herein. Sections 4.1-4.3 review measurements conducted in NCP, YRD and PRD, and measurements carried out in other regions in China are discussed in Section 4.4.

4.1 North China plain (NCP)

4.1.1 Beijing

In August-September 2006, size-resolved CCN activities were measured at the Yufa site (Gunthe et al., 2011). Maximum activation fractions were around 1 for supersaturation in the range of 0.26-0.86%; however, they only reached ~0.8 on average at 0.07% supersaturation, and these

841   inactive particles were mainly soot. For the entire measurement period, the average κ_a and κ_t were

842   both determined to be 0.3±0.1. CCN activities were found to increase with particle size due to

843   increased mass fractions of soluble inorganics (Gunthe et al., 2011), and κ_a was measured to be

844   ~0.2 at ~40 nm and ~0.5 at 200 nm. During periods affected by aged regional pollution, mass

845   fractions of soluble inorganics were enhanced, leading to increase in κ_a (0.35±0.05) (Gunthe et al.,

846   2011); in contrast, mass fractions of organics increased during periods influenced by fresh city

847   pollution, resulting in decrease in κ_a (0.22±0.07).
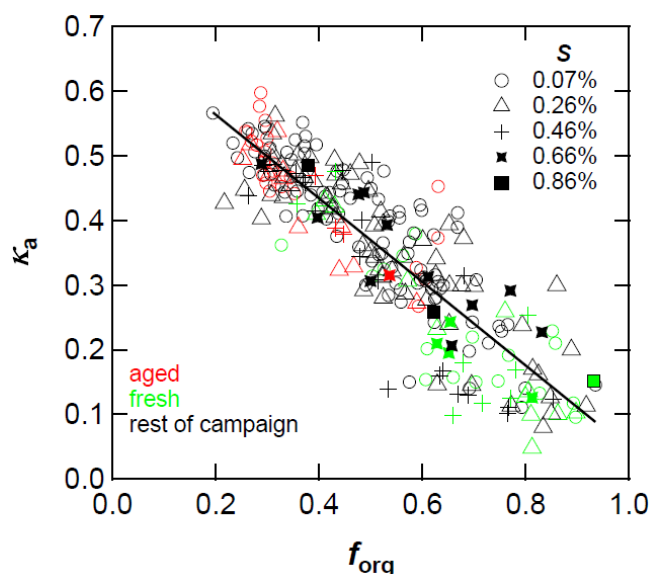
848

849   **Figure 6.** Dependence of κ_a on mass fractions of organics for three periods over the campaign (red:

850   the aged regional pollution period; green: the fresh city pollution period; black: the rest of the

851   campaign). Reprint with permission by Gunthe et al. (Gunthe et al., 2011). Copyright 2011

852   Copernicus Publications.

853

854   As shown in Figure 6, the measured CCN activities decreased as mass fractions of organics

855   increased (Gunthe et al., 2011); furthermore, the measured κ_a could be quantitatively described by

856   mass fractions of soluble inorganics and organics, and their κ were determined to be 0.7 and 0.1.

857   Aerosol CCN activities during a rapid particle growth event on 23 August were further examined

858   (Wiedensohler et al., 2009), during which CCN size distribution was dominated by the growing

859   nucleation mode instead of the accumulation mode in usual.

860   Measurements were carried out at the PKU site to investigate size-resolved CCN activities in

861   May-June 2014 (Wu et al., 2017). Similar to the concurrent H-TDMA measurements, average κ_a

862   was determined to be ~0.10 during biomass burning events, displaying no dependence on particles

863   size (Wu et al., 2017). CCN activities of submicrometer particles were significantly reduced during

864   biomass burning periods, due to increased mass fractions of organics and black carbon.

865   Furthermore, average κ calculated from aerosol compositions measured using AMS were

866   consistent with those derived from hygroscopic growth and CCN activity measurements (Wu et

867   al., 2017), if κ were assumed to be 0.53 and 0 for inorganics and organics.

868   Zhang et al. (Zhang et al., 2017) investigated size-resolved CCN activities at the IAP site in

869   November-December 2014 and August-September 2015, and maximum activation fractions were

870   found to be much smaller than one, indicating large fractions of CCN-inactive particles from local

871   primary emissions. The average κ_a, which ranged from 0.22 to 0.31 for 60-150 nm particles and

872   increased with particle size (Zhang et al., 2017), agreed well with those derived from the

873   concurrent H-TDMA measurements (Wang et al., 2017c). In addition, κ (0.32±0.11) calculated

874   using ACSM-measured aerosol composition were significantly larger than those derived from

875   hygroscopic growth (0.25±0.08) and CCN activities (0.26±0.04) (Zhang et al., 2017). This was

876   because hygroscopicity estimated using ASCM-measured composition did not consider the

877   contribution of smaller and less-hygroscopic particles (aerosol hygroscopicity became lower for

878   smaller particles, but ACSM only detected >60 nm particles).

879   In November-December 2016, Zhang et al. (Zhang et al., 2019a) further investigated size-

880   resolved CCN activities at the IAP site and found that [CCN] was significantly increased during

881   nucleation-initiated haze episodes. It was suggested that increase in particle size contributed >80%

882   to the observed increase in [CCN] (Ren et al., 2018; Zhang et al., 2019a), while the effect of aerosol

883   hygroscopicity enhancement, due to change in aerosol composition, was much smaller.

884   **4.1.2   Other locations in NCP**

885   Zhang et al. (Zhang et al., 2014; Zhang et al., 2017) measured size-resolved CCN activities at

886   the Xianghe site (39.75ºN, 116.96ºE) in June-July 2013. Average κ_a were determined to be 0.24-

887   0.32 during polluted periods, showing no dependence on particle size; in contrast, κ_a increased

888   from ~0.22 at ~50 nm to ~0.38 at ~180 nm for background days (Zhang et al., 2014). Compared

889   to polluted periods, κ_a were ~20% larger under background conditions for the accumulation mode

890   (100-200 nm), as the contribution of aerosol organics from fresh biomass burning was significantly

891   increased during pollution events (Zhang et al., 2014); however, κ_a were very similar for the

892   nucleation/Aitken modes (40-100 nm) under background and polluted conditions.

893   Size-resolved CCN activities were further investigated at Xianghe site in July-August 2013

894   (Ma et al., 2016; Tao et al., 2020), and it was found that κ_a increased with particle size, from

895   0.22±0.02 at 46 nm to 0.38±0.02 at 179 nm. Compared to that derived from concurrent H-TDMA

896   measurements, aerosol hygroscopicity derived from CCN activities were slightly lower for <50

897   nm particles but higher for >100 nm particles (Ma et al., 2016; Zhang et al., 2016b).

898   Zhang and co-workers (Zhang et al., 2016a; Li et al., 2017b; Zhang et al., 2017) also

899   investigated size-resolved CCN activities at the Xinzhou site in July-August 2014. The average κ_a

900   were determined to be 0.42-0.51 for 37-150 nm particles, exhibiting no dependence on particle

901   size (Zhang et al., 2017); compared to other sites in the NCP, aerosols at the Xinzhou site displayed

902   significantly higher CCN activities, as aerosols observed at this site were highly aged after

903   undergoing regional transport for a long time. The average κ_a (0.48±0.07) (Zhang et al., 2017)

904   agreed well with that (0.47±0.03) determined from concurrent H-TDMA measurements (Zhang et

905   al., 2017), both much significantly larger than that (0.41±0.06) calculated from ACSM-measured

906   aerosol composition, probably because such calculation may underestimate the hygroscopicity of

907   aerosol organics.

908   **4.2 Yangtze River Delta (YRD)**

909   Size-resolved CCN activity measurements were conducted in August 2013 at the NBM site

910   (32.04ºN. 118.70ºE) on the Jiangxi Island in the Yangtze River (Ma et al., 2017). This site, located

911   in a suburban area of Nanjing, did not have significant local emission at that time. The κ_a values

912   were found to range from ~0.1 to ~0.8 during the campaign, being 0.35±0.13 on average (Ma et

913   al., 2017), and no significant variation in average κ_a was found for biomass burning, urban, marine

914   and industrial air masses. In addition, κ_a increased from 0.30±0.08 at ~55 nm to 0.34±0.08 at 67

915   nm, due to larger contribution of low-hygroscopic organics at 50 nm; however, further increase in

916   particle size up to ~149 nm did not lead to obvious increase in κ_a (Ma et al., 2017), likely because

917   aerosols arriving at this site were heavily aged and well internally mixed.

918   Ling-term size-resolved CCN activities were studied in January-December 2013 at the Lin'an

919   site (Hangzhou, Zhejiang Province) (Che et al., 2016; Che et al., 2017), which is a WMO Global

920   Atmospheric Watch regional station (30.3ºN, 119.73ºE, 138 m above the sea level) located in the

921   center of YRD. Maximum activation fractions were close to one at high supersaturation but only

922   reached ~0.89 at 0.1% supersaturation. Values of κ_a and κ_t were almost identical (~0.25) at 40-50

923   nm and increased to ~0.42 (κ_a) and ~0.40 (κ_t) at 100-150 nm (Che et al., 2017), suggesting that

924   larger particles contained larger fractions of hygroscopic species (e.g., soluble inorganics).

925   Furthermore, CCN activities were also compared under nine different weather-pollution conditions

926   (Che et al., 2016), and κ were determined to be ~0.7 and ~0.1 for inorganics and organics during

927   haze episodes and ~0.6 and ~0.2 for other episodes.

928   **4.3 Pearl River Delta (PRD)**

929   Rose et al. (Rose et al., 2010; Rose et al., 2011) explored size-resolved CCN activities in July

930   2006 at the Backgarden site, which is a suburban site (23.55ºN, 113.07ºE) located ~60 km

931   northwest of Guangzhou. Maximum activation fractions were close to 1 at medium and high

932   supersaturation (0.47-1.27%) and well below 1 at low supersaturation (0.068-0.27%) (Rose et al.,

933   2010), and particles not activated were mainly externally mixed soot with an estimated median κ

934   of ~0.01 (Rose et al., 2011). The average κ_a and κ_t were determined to be 0.34 and 0.30 over the

935   entire campaign; to be more specific, κ_a and κ_t were almost identical (~0.3) for small particles and

936   increased to 0.4-0.5 and ~0.33 for large particles (Rose et al., 2010). Increase in average κ_a with

937   diameter was mainly due to enhanced mass fractions of inorganics for larger particles (Rose et al.,

938   2011). Compared to the rest of the campaign, κ_a and κ_t were reduced by ~30% on average during

939   biomass burning events (0.34 versus 0.24), when mass fractions of organics were substantially

940   increased; moreover, the decrease in κ_t during biomass burning events was very substantial for

941   <100 nm particles but quite small for ~200 nm particles (Rose et al., 2010). It was further found

942   that assuming κ to be ~0.6 for inorganics and ~0.1 for organics could approximate the observed

943   CCN activities over the entire campaign (Rose et al., 2011).

944   Size-resolved CCN activities were investigated at the Panyu site in November-December 2014

945   (Cai et al., 2018), and the average κ_a were found to increase from 0.21 at 58 nm to 0.30 at 156 nm,

946   because mass fractions of organics, measured using AMS, decreased with particle size. The

947   average κ derived from H-TDMA measurements agreed well with those derived from CCN

Atmospheric
Chemistry
and Physics
Discussions

Open Access

EGU

948   measurements; however, they were larger than those calculated from size-resolved chemical

949   compositions, and the difference between measured and calculated κ increased with particle size

950   (Cai et al., 2018). This discrepancy was probably because assuming a constant κ (0.1) may

951   underestimate the hygroscopicity of aerosol organics.

952   Aerosol CCN properties were studied at the HKUST site in May 2011 (Meng et al., 2014), and

953   maximum activation fractions were found to exceed 0.9 for the entire campaign, implying that the

954   difference between κ_a and κ_t should be small. CCN activities were found to increase with particle

955   size, with average κ_a being determined to be 0.28 at 46 nm to 0.39 at 116 nm (Meng et al., 2014),

956   due to increase in volume fractions of inorganics as revealed by AMS measurements. It was further

957   found that the measured κ_a could be reasonably well predicted using volume fractions of inorganics

958   and organics (Meng et al., 2014), and their κ were determined to be 0.6 and 0.1.

4.4 Other locations

960   Hung et al. (Hung et al., 2014; Hung et al., 2016) measured [CCN], [CN] and aerosol number

961   size distribution in August 2011 at a rural site and in June 2012 at an urban site in Taiwan. The

962   rural site (25.89ºN, 121.57ºE) is ~15 km away from Taipei, while the urban site (25.01ºN, 121.54ºE)

963   is located on the campus of National Taiwan University in a metropolitan area of Taipei. At the

964   rural site, κ_{cut} increased from ~0.1 at ~50 nm to ~0.35 at ~165 nm during the first period which

965   was significantly affected by anthropogenic emissions, while increased from ~0.04 at ~70 nm to

966   ~0.28 at ~175 nm for the second period not significantly affected by anthropogenic emissions

967   (Hung et al., 2014). Overall, κ_{cut} was larger in the first period than the second period, probably due

968   to the impacts of aged air masses originating from cities nearby during the first period. Compared

969   to the rural site, κ_{cut} were much smaller at the urban site, increasing from ~0.021 at ~90 nm to 0.10

970   at ~250 nm (Hung et al., 2016), indicating that fresh anthropogenic aerosols tended to exhibit lower

971   hygroscopicity.

972   Shipborne size-resolved CCN activity measurements were carried out in September 2012 over

973   remote regions of the South China Sea and East China Sea (Atwood et al., 2017). Under marine

974   background conditions, the average κ_a were determined to be 0.65±0.11 and 0.46±0.17 for the

975   accumulation and Aitken modes (Atwood et al., 2017). Compared to marine background

976   conditions, CCN activities were reduced after extensive precipitation, with average κ_a determined

977   to be 0.54±0.14 and 0.34±0.11 for the accumulation and Aitken modes; whereas during periods

978   impacted by biomass burning, κ_a was reduced to 0.40±0.03 for the accumulation mode but

979   increased instead to 0.56±0.25 for the Aitken mode (Atwood et al., 2017).

980   Size-resolved CCN activities were explored over north South China Sea (19º39'N to 22º43'N,

981   113º44'E to 118º12'E) in August 2018 (Cai et al., 2020), and no obvious dependence of κ_a on

982   particle size (50-100 nm) was observed. The campaign-averaged κ was determined to be ~0.40

983   (Cai et al., 2020), larger than these measured in the PRD region but smaller than those measured

984   over remote marine regions. This is because the air in north South China Sea was affected by both

985   continental air masses (low hygroscopicity) and marine background (high hygroscopicity).

986   **4.5 Summary**

987   Similar to H-TDMA measurements, CCN activity measurements in China were mainly carried

988   out in NCP, YRD and PRD, and almost all the measurements took place at or close to the ground

989   level. In addition, the number of CCN activity measurements is much smaller than H-TDMA

990   measurements. The limited number of field studies preclude any solid conclusions on diurnal and

991   seasonal variations of aerosol CCN activities being drawn.

992   Maximum activation fractions were typically found to be considerably smaller than 1 (Rose et

993   al., 2010; Gunthe et al., 2011; Che et al., 2017; Zhang et al., 2017), especially at low

994   supersaturation, and CCN-inactive particles were usually attributed to low hygroscopic primary

995   particles (e.g., soot) from local sources. The average κ, reported by previous studies, were

996   generally found to be in the range of 0.30-0.35; however, CCN activities could be significantly

997   reduced if measurement sites were affected by fresh urban pollution or biomass burning (Rose et

998   al., 2010; Gunthe et al., 2011; Zhang et al., 2014; Wu et al., 2017), due to enhanced contribution

999   of soot and organics. The average κ observed at the Xinzhou site appeared to be larger than those

1000   reported at other continental site (Zhang et al., 2017), probably because aerosols arriving at this

1001   site were heavily aged. In addition, two studies which investigated aerosol CCN activities in the

1002   marine boundary layer reported larger κ values (Atwood et al., 2017; Cai et al., 2020), compared

1003   to those at continental sites.
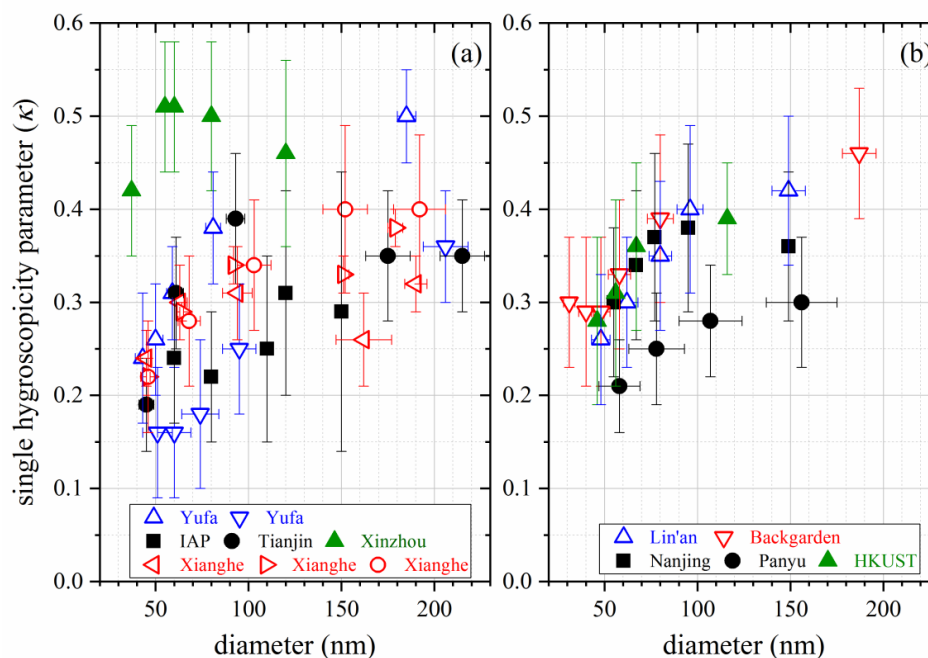
1004

1005 **Figure 7.** Measured κ_a as a function of particle diameter reported by previous studies (Rose et al.,

1006 2010; Deng et al., 2011; Gunthe et al., 2011; Deng et al., 2013; Meng et al., 2014; Zhang et al.,

1007 2014; Che et al., 2016; Ma et al., 2016; Che et al., 2017; Ma et al., 2017; Zhang et al., 2017; Cai

1008 et al., 2018; Tao et al., 2020) in the NCP (a) and other regions in China (b). Solid symbols represent

1009 urban/suburban sites, and open symbols represent rural sites.

1010

1011 Figure 7 summarizes size dependence of κ_a reported by CCN measurements at continental sites

1012 in China, and measurement data related to specific cases (e.g., biomass burning events) are not

1013 included (Rose et al., 2010; Wu et al., 2017). As shown in Figure 7, in general κ_a increased with

1014 particle size, as mass fractions increased with particle size for soluble inorganics and decreased for

1015 organics. Nevertheless, no obvious dependence of κ_a on particle size was also observed in Xinzhou

1016 (Zhang et al., 2017) and Nanjing (Ma et al., 2017), probably because aerosol particles at these two

1017 sites were substantially aged and thus very well internally mixed.

1018 Several studies carried out CCN activity closure analysis. Some studies suggested that the

1019 measured κ could be well quantitatively explained by aerosol composition (Rose et al., 2010;

1020 Gunthe et al., 2011; Wu et al., 2017), while other studies showed that κ estimated using aerosol

1021 composition were either larger (Zhang et al., 2017) or smaller than measured values (Zhang et al.,

1022 2017; Cai et al., 2018). In addition, a few studies investigated aerosol hygroscopic growth and

1023 CCN activities concurrently, and both consistence (Wu et al., 2017; Zhang et al., 2017; Cai et al.,

1024 2018) and discrepancies (Ma et al., 2016; Zhang et al., 2016b) were reported.

1025 **5 Perspectives**

1026 In the last 10-20 years a number of field measurements of hygroscopic properties and CCN

1027 activities of tropospheric aerosols have been carried out in China, and summaries of measured

1028   hygroscopic properties and CCN activities are provided in Sections 3.5 and 4.5. As shown in

1029   Sections 3 and 4, these studies have significantly improved our knowledge of tropospheric aerosol

1030   hygroscopicity in China and provided valuable data to better understand the roles aerosols play in

1031   heterogeneous and multiphase chemistry, as well as direct and indirect radiative forcing. However,

1032   large knowledge gaps still exist for aerosol hygroscopicity in China, as described below, and future

1033   research directions are also discussed.

1034   **Data availability:** In Tables S1-S5 we attempt to compile measurement data reported by

1035   previous studies under a consistent framework in order to enhance their accessibility and usability.

1036   However, important data are not always available from every study published; for example, several

1037   studies presented their main results graphically. It is recommended that in future data in the

1038   numerical form (H-TDMA measurements: including but not limited to diameter, RH, and GF

1039   and/or κ; CCN activity measurements: including but not limited to supersaturation, activation

1040   diameter and κ) should be provided.

1041   **Geographical coverages:** As shown in Sections 3-4, almost all the measurements of

1042   hygroscopic properties and CCN activities in China were carried out in east regions (e.g., NCP,

1043   YRD and PRD) heavily affected by anthropogenic emissions. Therefore, it will be very desirable

1044   in future to carry out these measurements in other regions; measurements in areas far from by

1045   human activities will be especially important, as they will provide information on aerosol

1046   hygroscopicity in the pristine troposphere.

1047   **Vertical distribution:** Most of previous aerosol hygroscopicity measurements in China were

1048   only carried out at or close to the ground level. However, both aerosol composition and RH, and

1049   as a result aerosol hygroscopic growth and CCN activation, will vary with altitude. For example,

1050   aircraft-based measurements of aerosol size distribution and composition indicated that single

hygroscopicity parameters would increase significantly with altitude (Liu et al., 2020), and it was

revealed from remote sensing that aerosol hygroscopicity at the upper boundary level was different

from that at the ground level (Tan et al., 2020). Therefore, in-situ measurements of vertical profiles

of aerosol composition and hygroscopicity on different platforms (e.g., towers, airships, aircrafts,

and etc.) will be very valuable; in addition, remote sensing may be very useful for retrieving

vertical profiles of aerosol hygroscopicity, as demonstrated by a very recent study (Tan et al., 2020).

Long-term measurements: Both aerosol concentration and composition have undergone (and

very likely will undergo) significant changes in China; however, most aerosol hygroscopicity

measurements were carried out for 1-2 months during specific field campaigns. Long-term

measurements of aerosol hygroscopicity will be very important to understand seasonal and annual

variations of aerosol hygroscopicity and the implications for visibility, atmospheric chemistry and

climate change.

Hygroscopicity of large particles: Tables S1-S4 reveal that the maximum aerosol diameter

examined in hygroscopic growth studies was 350 nm, which is the upper limit of dry aerosol size

for most of H-TDMA instruments (Tang et al., 2019). As particles larger than 350 nm can

contribute substantially to aerosol surface area and volume (or mass) concentrations,

hygroscopicity of these particles will be very important and should be measured in future, and this

requires technical improvements of H-TDMA. On the other hand, hygroscopicity of >350 nm

particles may not be very important for CCN activation, as these particles can be easily activated

due to their large diameters.

RH dependence: Most H-TDMA measurements were carried out at a single RH (usually

~90%), and a few studies which measured GF as a function of RH suggested that a constant κ

failed to describe hygroscopic growth at different RH. In addition, due to lack of measurement

Atmospheric
Chemistry
and Physics
Discussions

1074   data at different RH, it is not clear how well widely-used aerosol thermodynamic models can

1075   simulate ALWC at ambient RH. Therefore, measurements of aerosol hygroscopicity at different

1076   RH are certainly warranted.

1077   **The effect of aerosol organics:** As discussed in Section 3, several studies (Liu et al., 2014;

1078   Wu et al., 2016; Cai et al., 2018; Hong et al., 2018; Li et al., 2019b; Jin et al., 2020) suggested that

1079   organics contributed substantially to aerosol water uptake, while some studies also indicated that

1080   the contribution of aerosol organics to ALWC was rather minor. Therefore, aerosol hygroscopicity

1081   closure analysis, with concurrent measurements of aerosol composition and hygroscopicity, is

1082   recommended for future, in order to further understand the effects of aerosol organics on ALWC

1083   and CCN activation; in addition, relevant factors which need consideration include the dependence

1084   of hygroscopicity on composition of aerosol organics (e.g., O/C ratios) and the effects of aerosol

1085   organics on surface tension, phase separation effects, and etc.

1086

Reference

1103 Achtert, P., Birmili, W., Nowak, A., Wehner, B., Wiedensohler, A., Takegawa, N., Kondo, Y., Miyazaki, Y., Hu, M.,
1104 and Zhu, T.: Hygroscopic growth of tropospheric particle number size distributions over the North China Plain,
1105 Journal of Geophysical Research-Atmospheres, 114, D00G07, 10.1029/2008JD010921, 2009.
1106 An, Z., Huang, R.-J., Zhang, R., Tie, X., Li, G., Cao, J., Zhou, W., Shi, Z., Han, Y., Gu, Z., and Ji, Y.: Severe haze in
1107 northern China: A synergy of anthropogenic emissions and atmospheric processes, Proceedings of the National
1108 Academy of Sciences of the United States of America, 116, 8657-8666, 2019.
1109 Asmi, E., Frey, A., Virkkula, A., Ehn, M., Manninen, H. E., Timonen, H., Tolonen-Kivimaki, O., Aurela, M., Hillamo,
1110 R., and Kulmala, M.: Hygroscopicity and chemical composition of Antarctic sub-micrometre aerosol particles
1111 and observations of new particle formation, Atmospheric Chemistry and Physics, 10, 4253-4271, 2010.
1112 Atwood, S. A., Reid, J. S., Kreidenweis, S. M., Blake, D. R., Jonsson, H. H., Lagrosas, N. D., Xian, P., Reid, E. A.,
1113 Sessions, W. R., and Simpas, J. B.: Size-resolved aerosol and cloud condensation nuclei (CCN) properties in the
1114 remote marine South China Sea - Part 1: Observations and source classification, Atmospheric Chemistry and
1115 Physics, 17, 1105-1123, 2017.
1116 Bedoya-Velásquez, A. E., Navas-Guzmán, F., Jose Granados-Muñoz, M., Titos, G., Román, R., Andres Casquero-Vera,
1117 J., Ortiz-Amezcua, P., Antonio Benavent-Oltra, J., de Arruda Moreira, G., Montilla-Rosero, E., David Hoyos, C.,
1118 Artiñano, B., Coz, E., Jose Olmo-Reyes, F., Alados-Arboledas, L., and Luis Guerrero-Rascado, J.: Hygroscopic
1119 growth study in the framework of EARLINET during the SLOPE I campaign: synergy of remote sensing and in
1120 situ instrumentation, Atmospheric Chemistry and Physics, 18, 7001-7017, 2018.
1121 Bertram, T. H., and Thornton, J. A.: Toward a general parameterization of N2O5 reactivity on aqueous particles: the
1122 competing effects of particle liquid water, nitrate and chloride, Atmospheric Chemistry And Physics, 9, 8351-
1123 8363, 2009.
1124 Bian, Y. X., Zhao, C. S., Ma, N., Chen, J., and Xu, W. Y.: A study of aerosol liquid water content based on
1125 hygroscopicity measurements at high relative humidity in the North China Plain, Atmospheric Chemistry and
1126 Physics, 14, 6417-6426, 2014.
1127 Bougiatioti, A., Nenes, A., Fountoukis, C., Kalivitis, N., Pandis, S. N., and Mihalopoulos, N.: Size-resolved CCN
1128 distributions and activation kinetics of aged continental and marine aerosol, Atmospheric Chemistry and Physics,
1129 11, 8791-8808, 2011.
1130 Burgos, M. A., Andrews, E., Titos, G., Alados-Arboledas, L., Baltensperger, U., Day, D., Jefferson, A., Kalivitis, N.,
1131 Mihalopoulos, N., Sherman, J., Sun, J., Weingartner, E., and Zieger, P.: A global view on the effect of water
1132 uptake on aerosol particle light scattering, Scientific Data, 6, 157, 2019.
1133 Burkart, J., Steiner, G., Reischl, G., and Hitzenberger, R.: Long-term study of cloud condensation nuclei (CCN)
1134 activation of the atmospheric aerosol in Vienna, Atmospheric Environment, 45, 5751-5759, 2011.
1135 Cai, M., Tan, H., Chan, C. K., Mochida, M., Hatakeyama, S., Kondo, Y., Schurman, M. I., Xu, H., Li, F., Shimada, K.,
1136 Li, L., Deng, Y., Yai, H., Matsuki, A., Qin, Y., and Zhao, J.: Comparison of Aerosol Hygroscopcity, Volatility, and
1137 Chemical Composition between a Suburban Site in the Pearl River Delta Region and a Marine Site in Okinawa,
1138 Aerosol and Air Quality Research, 17, 3194-3208, 2017.
1139 Cai, M., Tan, H., Chan, C. K., Qin, Y., Xu, H., Li, F., Schurman, M. I., Liu, L., and Zhao, J.: The size-resolved cloud
1140 condensation nuclei (CCN) activity and its prediction based on aerosol hygroscopicity and composition in the
1141 Pearl Delta River (PRD) region during wintertime 2014, Atmospheric Chemistry and Physics, 18, 16419-16437,
1142 2018.

53

Cai, M., Liang, B., Sun, Q., Zhou, S., Yuan, B., Shao, M., Tan, H., and Zhao, J.: Effects of continental emissions on Cloud Condensation Nuclei (CCN) activity in northern South China Sea during summertime 2018, Atmospheric Chemistry and Physics Discussions, 2020, 1-43, 2020.

Cerully, K. M., Raatikainen, T., Lance, S., Tkacik, D., Tiitta, P., Petäjä, T., Ehn, M., Kulmala, M., Worsnop, D. R., Laaksonen, A., Smith, J. N., and Nenes, A.: Aerosol hygroscopicity and CCN activation kinetics in a boreal forest environment during the 2007 EUCAARI campaign, Atmos. Chem. Phys., 11, 12369-12386, 2011.

Che, H. C., Zhang, X. Y., Wang, Y. Q., Zhang, L., Shen, X. J., Zhang, Y. M., Ma, Q. L., Sun, J. Y., Zhang, Y. W., and Wang, T. T.: Characterization and parameterization of aerosol cloud condensation nuclei activation under different pollution conditions, Scientific reports, 6, 24497, 24410.21038/srep24497, 2016.

Che, H. C., Zhang, X. Y., Zhang, L., Wang, Y. Q., Zhang, Y. M., Shen, X. J., Ma, Q. L., Sun, J. Y., and Zhong, J. T.: Prediction of size-resolved number concentration of cloud condensation nuclei and long-term measurements of their activation characteristics, Scientific reports, 7, 5819, 5810.1038/s41598-41017-05998-41593, 2017.

Chen, H., Yang, S., Li, Y., Yin, Y., Zhang, Z., Yu, X., Kang, N., Yan, S., and Xia, H.: Hygroscopic Properties and Closure of Aerosol Chemical Composition in Mt. Huang in Summer (in Chinese), Environmental Science, 37, 2008-2016, 2016.

Chen, J., Li, Z., Lv, M., Wang, Y., Wang, W., Zhang, Y., Wang, H., Yan, X., Sun, Y., and Cribb, M.: Aerosol hygroscopic growth, contributing factors, and impact on haze events in a severely polluted region in northern China, Atmospheric Chemistry and Physics, 19, 1327-1342, 2019.

Chen, L. Y., Jeng, F. T., Chen, C. C., and Hsiao, T. C.: Hygroscopic behavior of atmospheric aerosol in Taipei, Atmospheric Environment, 37, 2069-2075, 2003.

Cheng, Y. F., Eichler, H., Wiedensohler, A., Heintzenberg, J., Zhang, Y. H., Hu, M., Herrmann, H., Zeng, L. M., Liu, S., Gnauk, T., Brueggemann, E., and He, L. Y.: Mixing state of elemental carbon and non-light-absorbing aerosol components derived from in situ particle optical properties at Xinken in Pearl River Delta of China, Journal of Geophysical Research-Atmospheres, 111, D20204, 20210.21029/22005JD006929, 2006.

Cheung, H. H. Y., Yeung, M. C., Li, Y. J., Lee, B. P., and Chan, C. K.: Relative Humidity- Dependent HTDMA Measurements of Ambient Aerosols at the HKUST Supersite in Hong Kong, China, Aerosol Science and Technology, 49, 643-654, 2015.

Chu, B. W., Ma, Q. X., Duan, F. K., Ma, J. Z., Jiang, J. K., He, K. B., and He, H.: Atmospheric "Haze Chemistry": Concept and Research Prospects, Progress in Chemistry, 32, 1-4, 2020.

Chuang, P. Y., Nenes, A., Smith, J. N., Flagan, R. C., and Seinfeld, J. H.: Design of a CCN instrument for airborne measurement, Journal of Atmospheric and Oceanic Technology, 17, 1005-1019, 2000.

Cocker, D. R., Whitlock, N. E., Flagan, R. C., and Seinfeld, J. H.: Hygroscopic properties of Pasadena, California aerosol, Aerosol Science and Technology, 35, 637-647, 2001.

Cubison, M. J., Coe, H., and Gysel, M.: A modified hygroscopic tandem DMA and a data retrieval method based on optimal estimation, Journal of Aerosol Science, 36, 846-865, 2005.

Dawson, K. W., Ferrare, R. A., Moore, R. H., Clayton, M. B., Thorsen, T. J., and Eloranta, E. W.: Ambient Aerosol Hygroscopic Growth From Combined Raman Lidar and HSRL, Journal of Geophysical Research-Atmospheres, 125, 031708, 031710.031029/032019JD031708, 2020.

Deng, Z. Z., Zhao, C. S., Ma, N., Liu, P. F., Ran, L., Xu, W. Y., Chen, J., Liang, Z., Liang, S., Huang, M. Y., Ma, X. C., Zhang, Q., Quan, J. N., Yan, P., Henning, S., Mildenberger, K., Sommerhage, E., Schaefer, M., Stratmann, F., and Wiedensohler, A.: Size-resolved and bulk activation properties of aerosols in the North China Plain, Atmospheric Chemistry and Physics, 11, 3835-3846, 2011.

Deng, Z. Z., Zhao, C. S., Ma, N., Ran, L., Zhou, G. Q., Lu, D. R., and Zhou, X. J.: An examination of parameterizations for the CCN number concentration based on in situ measurements of aerosol activation properties in the North China Plain, Atmospheric Chemistry and Physics, 13, 6227-6237, 2013.

Ding, J., Zhang, Y. F., Zhao, P. S., Tang, M., Xiao, Z. M., Zhang, W. H., Zhang, H. T., Yu, Z. J., Du, X., Li, L. W., Yuan, J., and Feng, Y. C.: Comparison of size-resolved hygroscopic growth factors of urban aerosol by different methods in Tianjin during a haze episode, Science of the Total Environment, 678, 618-626, 2019.

Duan, J., Tao, J., Wu, Y., Cheng, T., Zhang, R., Wang, Y., Zhu, H., Xie, X., Liu, Y., Li, X., Kong, L., Li, M., and He, Q.: Comparison of aerosol and cloud condensation nuclei between wet and dry seasons in Guangzhou, southern China, Science of the Total Environment, 607, 11-22, 2017.

Duan, J., Wang, Y., Xie, X., Li, M., Tao, J., Wu, Y., Cheng, T., Zhang, R., Liu, Y., Li, X., He, Q., Gao, W., and Wang, J.: Influence of pollutants on activity of aerosol cloud condensation nuclei (CCN) during pollution and post-rain periods in Guangzhou, southern China, Science of the Total Environment, 642, 1008-1019, 2018.

Duplissy, J., Gysel, M., Sjogren, S., Meyer, N., Good, N., Kammermann, L., Michaud, V., Weigel, R., dos Santos, S. M., Gruening, C., Villani, P., Laj, P., Sellegri, K., Metzger, A., McFiggans, G. B., Wehrle, G., Richter, R.,

54

1199   Dommen, J., Ristovski, Z., Baltensperger, U., and Weingartner, E.: Intercomparison study of six HTDMAs:
1200   results and recommendations, Atmospheric Measurement Techniques, 2, 363-378, 2009.
1201 Dusek, U., Frank, G. P., Hildebrandt, L., Curtius, J., Schneider, J., Walter, S., Chand, D., Drewnick, F., Hings, S., Jung,
1202   D., Borrmann, S., and Andreae, M. O.: Size matters more than chemistry for cloud-nucleating ability of aerosol
1203   particles, Science, 312, 1375-1378, 2006.
1204 Eichler, H., Cheng, Y. F., Birmili, W., Nowak, A., Wiedensohler, A., Brueggemann, E., Gnauk, T., Herrmann, H.,
1205   Althausen, D., Ansmann, A., Engelmann, R., Tesche, M., Wendisch, M., Zhang, Y. H., Hu, M., Liu, S., and Zeng,
1206   L. M.: Hygroscopic properties and extinction of aerosol particles at ambient relative humidity in South-Eastern
1207   China, Atmospheric Environment, 42, 6321-6334, 2008.
1208 Fajardo, O. A., Jiang, J., and Hao, J.: Continuous Measurement of Ambient Aerosol Liquid Water Content in Beijing,
1209   Aerosol and Air Quality Research, 16, 1152-1164, 2016.
1210 Fan, X., Liu, J., Zhang, F., Chen, L., Collins, D., Xu, W., Jin, X., Ren, J., Wang, Y., Wu, H., Li, S., Sun, Y., and Li, Z.:
1211   Contrasting size-resolved hygroscopicity of fine particles derived by HTDMA and HR-ToF-AMS measurements
1212   between summer and winter in Beijing: the impacts of aerosol aging and local emissions, Atmospheric Chemistry
1213   and Physics, 20, 915-929, 2020.
1214 Fang, S., Han, Y., Chen, K., Lu, C., Yin, Y., Tan, H., and Wang, J.: Parameterization and comparative evaluation of
1215   the CCN number concentration on Mt. Huang, China, Atmospheric Research, 181, 300-311, 2016.
1216 Farmer, D. K., Cappa, C. D., and Kreidenweis, S. M.: Atmospheric processes and their controlling influence on cloud
1217   condensation nuclei activity, Chem Rev, 115, 4199-4217, 2015.
1218 Frank, G. P., Dusek, U., and Andreae, M. O.: Technical note: Characterization of a static thermal-gradient CCN counter,
1219   Atmospheric Chemistry and Physics, 7, 3071-3080, 2007.
1220 Fukuta, N., and Saxena, V. K.: HORIZONTAL THERMAL-GRADIENT CLOUD CONDENSATION NUCLEUS
1221   SPECTROMETER, Journal of Applied Meteorology, 18, 1352-1362, 1979.
1222 Gao, Y., Zhang, D., Wang, J., Gao, H., and Yao, X.: Variations in Ncn and Nccn over China marginal seas related to
1223   marine traffic emissions, new particle formation and aerosol aging, Atmospheric Chemistry and Physics
1224   Discussions, 2020, 1-37, 2020.
1225 Good, N., Coe, H., and McFiggans, G.: Instrumentational operation and analytical methodology for the reconciliation
1226   of aerosol water uptake under sub- and supersaturated conditions, Atmospheric Measurement Techniques, 3,
1227   1241-1254, 2010.
1228 Gunthe, S. S., Rose, D., Su, H., Garland, R. M., Achtert, P., Nowak, A., Wiedensohler, A., Kuwata, M., Takegawa, N.,
1229   Kondo, Y., Hu, M., Shao, M., Zhu, T., Andreae, M. O., and Poeschl, U.: Cloud condensation nuclei (CCN) from
1230   fresh and aged air pollution in the megacity region of Beijing, Atmospheric Chemistry and Physics, 11, 11023-
1231   11039, 2011.
1232 Guo, S., Hu, M., Zamora, M. L., Peng, J., Shang, D., Zheng, J., Du, Z., Wu, Z., Shao, M., and Zeng, L.: Elucidating
1233   severe urban haze formation in China, Proceedings of the National Academy of Sciences, 111, 17373-17378,
1234   2014.
1235 Gysel, M., Crosier, J., Topping, D. O., Whitehead, J. D., Bower, K. N., Cubison, M. J., Williams, P. I., Flynn, M. J.,
1236   McFiggans, G. B., and Coe, H.: Closure study between chemical composition and hygroscopic growth of aerosol
1237   particles during TORCH2, Atmospheric Chemistry and Physics, 7, 6131-6144, 2007.
1238 Gysel, M., McFiggans, G. B., and Coe, H.: Inversion of tandem differential mobility analyser (TDMA) measurements,
1239   Journal of Aerosol Science, 40, 134-151, 2009.
1240 He, H., Wang, Y., Ma, Q., Ma, J., Chu, B., Ji, D., Tang, G., Liu, C., Zhang, H., and Hao, J.: Mineral dust and NOx
1241   promote the conversion of SO2 to sulfate in heavy pollution days, Scientific reports, 4, 4172, 2014.
1242 Hong, J., Xu, H., Tan, H., Yin, C., Hao, L., Li, F., Cai, M., Deng, X., Wang, N., Su, H., Cheng, Y., Wang, L., Petaja,
1243   T., and Kerminen, V.-M.: Mixing state and particle hygroscopicity of organic-dominated aerosols over the Pearl
1244   River Delta region in China, Atmospheric Chemistry and Physics, 18, 14079-14094, 2018.
1245 Huang, R.-J., Zhang, Y., Bozzetti, C., Ho, K.-F., Cao, J.-J., Han, Y., Daellenbach, K. R., Slowik, J. G., Platt, S. M.,
1246   and Canonaco, F.: High secondary aerosol contribution to particulate pollution during haze events in China,
1247   Nature, 514, 218, 2014.
1248 Hudson, J. G.: AN INSTANTANEOUS CCN SPECTROMETER, Journal of Atmospheric and Oceanic Technology,
1249   6, 1055-1065, 1989.
1250 Hung, H.-M., Lu, W.-J., Chen, W.-N., Chang, C.-C., Chou, C. C. K., and Lin, P.-H.: Enhancement of the hygroscopicity
1251   parameter kappa of rural aerosols in northern Taiwan by anthropogenic emissions, Atmospheric Environment,
1252   84, 78-87, 2014.

Hung, H.-M., Hsu, C.-H., Lin, W.-T., and Chen, Y.-Q.: A case study of single hygroscopicity parameter and its link to the functional groups and phase transition for urban aerosols in Taipei City, Atmospheric Environment, 132, 240-248, 2016.

Ji, Q., Shaw, G. E., and Cantrell, W.: A new instrument for measuring cloud condensation nuclei: Cloud condensation nucleus "remover", Journal of Geophysical Research-Atmospheres, 103, 28013-28019, 1998.

Jiang, R., Tan, H., Tang, L., Cai, M., Yin, Y., Li, F., Liu, L., Xu, H., Chan, P. W., Deng, X., and Wu, D.: Comparison of aerosol hygroscopicity and mixing state between winter and summer seasons in Pearl River Delta region, China, Atmospheric Research, 169, 160-170, 2016.

Jin, X., Wang, Y., Li, Z., Zhang, F., Xu, W., Sun, Y., Fan, X., Chen, G., Wu, H., Ren, J., Wang, Q., and Cribb, M.: Significant contribution of organics to aerosol liquid water content in winter in Beijing, China, Atmospheric Chemistry and Physics, 20, 901-914, 2020.

Kim, J.-S., Kim, Y. J., and Park, K.: Measurements of hygroscopicity and volatility of atmospheric ultrafine particles in the rural Pearl River Delta area of China, Atmospheric Environment, 45, 4661-4670, 2011.

King, S. M., Rosenoern, T., Shilling, J. E., Chen, Q., and Martin, S. T.: Increased cloud activation potential of secondary organic aerosol for atmospheric mass loadings, Atmospheric Chemistry and Physics, 9, 2959-2971, 2009.

Kreidenweis, S. M., Koehler, K., DeMott, P. J., Prenni, A. J., Carrico, C., and Ervens, B.: Water activity and activation diameters from hygroscopicity data - Part I: Theory and application to inorganic salts, Atmospheric Chemistry and Physics, 5, 1357-1370, 2005.

Kreidenweis, S. M., and Asa-Awuku, A.: 5.13 - Aerosol Hygroscopicity: Particle Water Content and Its Role in Atmospheric Processes, in: Treatise on Geochemistry (Second Edition), edited by: Turekian, K. K., Elsevier, Oxford, 331-361, 2014.

Kuang, Y., Zhao, C., Tao, J., Bian, Y., Ma, N., and Zhao, G.: A novel method for deriving the aerosol hygroscopicity parameter based only on measurements from a humidified nephelometer system, Atmospheric Chemistry and Physics, 17, 6651-6662, 2017.

Kuang, Y., Zhao, C. S., Zhao, G., Tao, J. C., Xu, W., Ma, N., and Bian, Y. X.: A novel method for calculating ambient aerosol liquid water content based on measurements of a humidified nephelometer system, Atmospheric Measurement Techniques, 11, 2967-2982, 2018.

Lance, S., Medina, J., Smith, J. N., and Nenes, A.: Mapping the operation of the DMT Continuous Flow CCN counter, Aerosol Science and Technology, 40, 242-254, 2006.

Leng, C., Cheng, T., Chen, J., Zhang, R., Tao, J., Huang, G., Zha, S., Zhang, M., Fang, W., Li, X., and Li, L.: Measurements of surface cloud condensation nuclei and aerosol activity in downtown Shanghai, Atmospheric Environment, 69, 354-361, 2013.

Leng, C., Zhang, Q., Zhang, D., Xu, C., Cheng, T., Zhang, R., Tao, J., Chen, J., Zha, S., Zhang, Y., Li, X., Kong, L., and Gao, W.: Variations of cloud condensation nuclei (CCN) and aerosol activity during fog-haze episode: a case study from Shanghai, Atmospheric Chemistry and Physics, 14, 12499-12512, 2014.

Li, K., Zhu, Y., Gao, H., and Yao, X.: A comparative study of cloud condensation nuclei measured between non-heating and heating periods at a suburb site of Qingdao in the North China, Atmospheric Environment, 112, 40-53, 2015a.

Li, K., Ye, X., Pang, H., Lu, X., Chen, H., Wang, X., Yang, X., Chen, J., and Chen, Y.: Temporal variations in the hygroscopicity and mixing state of black carbon aerosols in a polluted megacity area, Atmospheric Chemistry and Physics, 18, 15201-15218, 2018.

Li, K., Jacob, D. J., Liao, H., Shen, L., Zhang, Q., and Bates, K. H.: Anthropogenic drivers of 2013-2017 trends in summer surface ozone in China, Proceedings of the National Academy of Sciences of the United States of America, 116, 422-427, 2019a.

Li, M., Liu, H., Geng, G., Hong, C., Liu, F., Song, Y., Tong, D., Zheng, B., Cui, H., Man, H., Zhang, Q., and He, K.: Anthropogenic emission inventories in China: a review, National Science Review, 4, 834-866, 2017a.

Li, Q., Yin, Y., Gu, X., Yuan, L., Kong, S., Jiang, Q., Chen, K., and Li, L.: An observational study of aerosol hygroscopic growth factor and cloud condensation nuclei in Nanjing in summer (in Chinese), China Environmental Science, 35, 337-346, 2015b.

Li, W., Shao, L., Zhang, D., Ro, C.-U., Hu, M., Bi, X., Geng, H., Matsuki, A., Niu, H., and Chen, J.: A review of single aerosol particle studies in the atmosphere of East Asia: morphology, mixing state, source, and heterogeneous reactions, Journal of Cleaner Production, 112, 1330-1349, 2016.

Li, X., Song, S., Zhou, W., Hao, J., Worsnop, D. R., and Jiang, J.: Interactions between aerosol organic components and liquid water content during haze episodes in Beijing, Atmospheric Chemistry and Physics, 19, 12163-12174, 2019b.

1309   Li, Y., Zhang, F., Li, Z., Sun, L., Wang, Z., Li, P., Sun, Y., Ren, J., Wang, Y., Cribb, M., and Yuan, C.: Influences of
1310   aerosol physiochemical properties and new particle formation on CCN activity from observation at a suburban
1311   site of China, Atmospheric Research, 188, 80-89, 2017b.
1312   Liu, B. Y. H., Pui, D. Y. H., Whitby, K. T., Kittelson, D. B., Kousaka, Y., and McKenzie, R. L.: AEROSOL MOBILITY
1313   CHROMATOGRAPH - NEW DETECTOR FOR SULFURIC-ACID AEROSOLS, Atmospheric Environment,
1314   12, 99-104, 1978.
1315   Liu, H. J., Zhao, C. S., Nekat, B., Ma, N., Wiedensohler, A., van Pinxteren, D., Spindler, G., Mueller, K., and Herrmann,
1316   H.: Aerosol hygroscopicity derived from size-segregated chemical composition and its parameterization in the
1317   North China Plain, Atmospheric Chemistry and Physics, 14, 2525-2539, 2014.
1318   Liu, L., Tan, H., Fan, S., Cai, M., Xu, H., Li, F., and Chan, P.: Influence of aerosol hygroscopicity and mixing state on
1319   aerosol optical properties in the Pearl River Delta region, China, Science of the Total Environment, 627, 1560-
1320   1571, 2018.
1321   Liu, P. F., Zhao, C. S., Goebel, T., Hallbauer, E., Nowak, A., Ran, L., Xu, W. Y., Deng, Z. Z., Ma, N., Mildenberger,
1322   K., Henning, S., Stratmann, F., and Wiedensohler, A.: Hygroscopic properties of aerosol particles at high relative
1323   humidity and their diurnal variations in the North China Plain, Atmospheric Chemistry and Physics, 11, 3479-
1324   3494, 2011.
1325   Liu, Q., Liu, D., Gao, Q., Tian, P., Wang, F., Zhao, D., Bi, K., Wu, Y., Ding, S., Hu, K., Zhang, J., Ding, D., and Zhao,
1326   C.: Vertical characteristics of aerosol hygroscopicity and impacts on optical properties over the North China Plain
1327   during winter, Atmospheric Chemistry and Physics, 20, 3931-3944, 2020.
1328   Liu, Y., Wu, Z., Wang, Y., Xiao, Y., Gu, F., Zheng, J., Tan, T., Shang, D., Wu, Y., Zeng, L., Hu, M., Bateman, A. P.,
1329   and Martin, S. T.: Submicrometer Particles Are in the Liquid State during Heavy Haze Episodes in the Urban
1330   Atmosphere of Beijing, China, Environmental Science & Technology Letters, 4, 427-432, 2017.
1331   Lopez-Yglesias, X. F., Yeung, M. C., Dey, S. E., Brechtel, F. J., and Chan, C. K.: Performance Evaluation of the
1332   Brechtel Mfg. Humidified Tandem Differential Mobility Analyzer (BMI HTDMA) for Studying Hygroscopic
1333   Properties of Aerosol Particles, Aerosol Science and Technology, 48, 969-980, 2014.
1334   Lu, G., and Guo, X.: Distribution and origin of aerosol and its transform relationship with CCN derived from the
1335   spring multi-aircraft measurements of Beijing Cloud Experiment (BCE), Chinese Science Bulletin, 57, 2460-
1336   2469, 2012.
1337   Lu, K., Guo, S., Tan, Z., Wang, H., Shang, D., Liu, Y., Li, X., Wu, Z., Hu, M., and Zhang, Y.: Exploring atmospheric
1338   free-radical chemistry in China: the self-cleansing capacity and the formation of secondary air pollution, National
1339   Science Review, 6, 579-594, 2019.
1340   Lu, X., Zhang, L., Wang, X., Gao, M., Li, K., Zhang, Y., Yue, X., and Zhang, Y.: Rapid Increases in Warm-Season
1341   Surface Ozone and Resulting Health Impact in China Since 2013, Environmental Science & Technology Letters,
1342   7, 240-247, 2020.
1343   Lv, M., Liu, D., Li, Z., Mao, J., Sun, Y., Wang, Z., Wang, Y., and Xie, C.: Hygroscopic growth of atmospheric aerosol
1344   particles based on lidar, radiosonde, and in situ measurements: Case studies from the Xinzhou field campaign,
1345   Journal of Quantitative Spectroscopy & Radiative Transfer, 188, 60-70, 2017.
1346   Ma, N., Zhao, C., Tao, J., Wu, Z., Kecorius, S., Wang, Z., Groess, J., Liu, H., Bian, Y., Kuang, Y., Teich, M., Spindler,
1347   G., Mueller, K., van Pinxteren, D., Herrmann, H., Hu, M., and Wiedensohler, A.: Variation of CCN activity during
1348   new particle formation events in the North China Plain, Atmospheric Chemistry and Physics, 16, 8593-8607,
1349   2016.
1350   Ma, Y., Li, S., Zheng, J., Khalizov, A., Wang, X., Wang, Z., and Zhou, Y.: Size-resolved measurements of mixing state
1351   and cloud-nucleating ability of aerosols in Nanjing, China, Journal of Geophysical Research-Atmospheres, 122,
1352   9430-9450, 2017.
1353   Massling, A., Stock, M., Wehner, B., Wu, Z. J., Hu, M., Brueggemann, E., Gnauk, T., Herrmann, H., and Wiedensohler,
1354   A.: Size segregated water uptake of the urban submicrometer aerosol in Beijing, Atmospheric Environment, 43,
1355   1578-1589, 2009.
1356   Massling, A., Niedermeier, N., Hennig, T., Fors, E. O., Swietlicki, E., Ehn, M., Hameri, K., Villani, P., Laj, P., Good,
1357   N., McFiggans, G., and Wiedensohler, A.: Results and recommendations from an intercomparison of six
1358   Hygroscopicity-TDMA systems, Atmospheric Measurement Techniques, 4, 485-497, 2011.
1359   McFiggans, G., Artaxo, P., Baltensperger, U., Coe, H., Facchini, M. C., Feingold, G., Fuzzi, S., Gysel, M., Laaksonen,
1360   A., Lohmann, U., Mentel, T. F., Murphy, D. M., O'Dowd, C. D., Snider, J. R., and Weingartner, E.: The effect of
1361   physical and chemical aerosol properties on warm cloud droplet activation, Atmos. Chem. Phys., 6, 2593-2649,
1362   2006.
1363   McMurry, P. H., Takano, H., and Anderson, G. R.: STUDY OF THE AMMONIA (GAS) SULFURIC-ACID
1364   (AEROSOL) REACTION-RATE, Environmental Science & Technology, 17, 347-352, 1983.

1365 McMurry, P. H., and Stolzenburg, M. R.: ON THE SENSITIVITY OF PARTICLE-SIZE TO RELATIVE-HUMIDITY
1366   FOR LOS-ANGELES AEROSOLS, Atmospheric Environment, 23, 497-507, 1989.
1367 McMurry, P. H.: A review of atmospheric aerosol measurements, Atmospheric Environment, 34, 1959-1999, 2000.
1368 Meier, J., Wehner, B., Massling, A., Birmili, W., Nowak, A., Gnauk, T., Brueggemann, E., Herrmann, H., Min, H., and
1369   Wiedensohler, A.: Hygroscopic growth of urban aerosol particles in Beijing (China) during wintertime: a
1370   comparison of three experimental methods, Atmospheric Chemistry and Physics, 9, 6865-6880, 2009.
1371 Meng, J. W., Yeung, M. C., Li, Y. J., Lee, B. Y. L., and Chan, C. K.: Size-resolved cloud condensation nuclei (CCN)
1372   activity and closure analysis at the HKUST Supersite in Hong Kong, Atmospheric Chemistry and Physics, 14,
1373   10267-10282, 2014.
1374 Moore, R. H., Nenes, A., and Medina, J.: Scanning Mobility CCN Analysis-A Method for Fast Measurements of Size-
1375   Resolved CCN Distributions and Activation Kinetics, Aerosol Science and Technology, 44, 861-871, 2010.
1376 Nenes, A., Chuang, P. Y., Flagan, R. C., and Seinfeld, J. H.: A theoretical analysis of cloud condensation nucleus (CCN)
1377   instruments, Journal of Geophysical Research-Atmospheres, 106, 3449-3474, 2001.
1378 Otto, P., Georgii, H. W., and Bingemer, H.: A new three-stage continuous flow CCN-counter, Atmospheric Research,
1379   61, 299-310, 2002.
1380 Petters, M. D., and Kreidenweis, S. M.: A single parameter representation of hygroscopic growth and cloud
1381   condensation nucleus activity, Atmospheric Chemistry And Physics, 7, 1961-1971, 2007.
1382 Petters, M. D., Prenni, A. J., Kreidenweis, S. M., and DeMott, P. J.: On measuring the critical diameter of cloud
1383   condensation nuclei using mobility selected aerosol, Aerosol Science and Technology, 41, 907-913, 2007.
1384 Petters, M. D., Carrico, C. M., Kreidenweis, S. M., Prenni, A. J., DeMott, P. J., Collett, J. L., Jr., and Moosmueller, H.:
1385   Cloud condensation nucleation activity of biomass burning aerosol, Journal of Geophysical Research-
1386   Atmospheres, 114, 2009.
1387 Qian, X., Zhang, Q., Xu, X., Fang, B., Zhao, W., Bao, J., and Zhang, W.: Development of a Volatility Hygroscopic
1388   Tandem Differential Mobility Analyzer (VH-TDMA) for the measurement of aerosol thermal and hygroscopic
1389   properties (in Chinese), China Environmental Science, 37, 1269-1275, 2017.
1390 Rader, D. J., and McMurry, P. H.: APPLICATION OF THE TANDEM DIFFERENTIAL MOBILITY ANALYZER
1391   TO STUDIES OF DROPLET GROWTH OR EVAPORATION, Journal of Aerosol Science, 17, 771-787, 1986.
1392 Ren, J., Zhang, F., Wang, Y., Collins, D., Fan, X., Jin, X., Xu, W., Sun, Y., Cribb, M., and Li, Z.: Using different
1393   assumptions of aerosol mixing state and chemical composition to predict CCN concentrations based on field
1394   measurements in urban Beijing, Atmospheric Chemistry and Physics, 18, 6907-6921, 2018.
1395 Riemer, N., Ault, A. P., West, M., Craig, R. L., and Curtis, J. H.: Aerosol Mixing State: Measurements, Modeling, and
1396   Impacts, Reviews of Geophysics, 57, 187-249, 2019.
1397 Roberts, G. C., and Nenes, A.: A continuous-flow streamwise thermal-gradient CCN chamber for atmospheric
1398   measurements, Aerosol Science and Technology, 39, 206-221, 2005.
1399 Rose, D., Gunthe, S. S., Mikhailov, E., Frank, G. P., Dusek, U., Andreae, M. O., and Poeschl, U.: Calibration and
1400   measurement uncertainties of a continuous-flow cloud condensation nuclei counter (DMT-CCNC): CCN
1401   activation of ammonium sulfate and sodium chloride aerosol particles in theory and experiment, Atmospheric
1402   Chemistry and Physics, 8, 1153-1179, 2008.
1403 Rose, D., Nowak, A., Achtert, P., Wiedensohler, A., Hu, M., Shao, M., Zhang, Y., Andreae, M. O., and Poeschl, U.:
1404   Cloud condensation nuclei in polluted air and biomass burning smoke near the mega-city Guangzhou, China -
1405   Part 1: Size-resolved measurements and implications for the modeling of aerosol particle hygroscopicity and
1406   CCN activity, Atmospheric Chemistry and Physics, 10, 3365-3383, 2010.
1407 Rose, D., Gunthe, S. S., Su, H., Garland, R. M., Yang, H., Berghof, M., Cheng, Y. F., Wehner, B., Achtert, P., Nowak,
1408   A., Wiedensohler, A., Takegawa, N., Kondo, Y., Hu, M., Zhang, Y., Andreae, M. O., and Poeschl, U.: Cloud
1409   condensation nuclei in polluted air and biomass burning smoke near the mega-city Guangzhou, China -Part 2:
1410   Size-resolved aerosol chemical composition, diurnal cycles, and externally mixed weakly CCN-active soot
1411   particles, Atmospheric Chemistry and Physics, 11, 2817-2836, 2011.
1412 Sinnarwalla, A. M., and Alofs, D. J.: A cloud nucleus counter with long available growth time, Journal of Applied
1413   Meteorology, 12, 831-835, 1973.
1414 Sjogren, S., Gysel, M., Weingartner, E., Alfarra, M. R., Duplissy, J., Cozic, J., Crosier, J., Coe, H., and Baltensperger,
1415   U.: Hygroscopicity of the submicrometer aerosol at the high-alpine site Jungfraujoch, 3580 m a.s.l., Switzerland,
1416   Atmospheric Chemistry and Physics, 8, 5715-5729, 2008.
1417 Snider, J. R., Petters, M. D., Wechsler, P., and Liu, P. S. K.: Supersaturation in the Wyoming CCN instrument, Journal
1418   of Atmospheric and Oceanic Technology, 23, 1323-1339, 2006.
1419 Stolzenburg, M. R., and McMurry, P. H.: TDMAfit User's Manual, Particle Technology Laboratory, Department of
1420   Mechanical Engineering, University of Minnesota, Minneapolis, MN 55455, 1988.

Stratmann, F., Kauffeldt, T., Hummes, D., and Fissan, H.: Differential electrical mobility analysis: A theoretical study, Aerosol Science and Technology, 26, 368-383, 1997.

Sullivan, R. C., Moore, M. J. K., Petters, M. D., Kreidenweis, S. M., Roberts, G. C., and Prather, K. A.: Effect of chemical mixing state on the hygroscopicity and cloud nucleation properties of calcium mineral dust particles, Atmospheric Chemistry and Physics, 9, 3303-3316, 2009.

Svenningsson, B., Rissler, J., Swietlicki, E., Mircea, M., Bilde, M., Facchini, M. C., Decesari, S., Fuzzi, S., Zhou, J., Monster, J., and Rosenorn, T.: Hygroscopic growth and critical supersaturations for mixed aerosol particles of inorganic and organic compounds of atmospheric relevance, Atmospheric Chemistry and Physics, 6, 1937-1952, 2006.

Swietlicki, E., Hansson, H. C., Hameri, K., Svenningsson, B., Massling, A., McFiggans, G., McMurry, P. H., Petaja, T., Tunved, P., Gysel, M., Topping, D., Weingartner, E., Baltensperger, U., Rissler, J., Wiedensohler, A., and Kulmala, M.: Hygroscopic properties of submicrometer atmospheric aerosol particles measured with H-TDMA instruments in various environments - a review, Tellus Series B-Chemical and Physical Meteorology, 60, 432-469, 2008.

Tan, H., Yin, Y., Gu, X., Li, F., Chan, P. W., Xu, H., Deng, X., and Wan, Q.: An observational study of the hygroscopic properties of aerosols over the Pearl River Delta region, Atmospheric Environment, 77, 817-826, 2013.

Tan, H., Cai, M., Fan, Q., Liu, L., Li, F., Chan, P. W., Deng, X., and Wu, D.: An analysis of aerosol liquid water content and related impact factors in Pearl River Delta, Science of the Total Environment, 579, 1822-1830, 2017.

Tan, W., Yu, Y., Li, C., Li, J., Kang, L., Dong, H., Zeng, L., and Zhu, T.: Profiling Aerosol Liquid Water Content Using a Polarization Lidar, Environmental Science & Technology, 54, 3129-3137, 2020.

Tan, Z., Rohrer, F., Lu, K., Ma, X., Bohn, B., Broch, S., Dong, H., Fuchs, H., Gkatzelis, G. I., Hofzumahaus, A., Holland, F., Li, X., Liu, Y., Liu, Y., Novelli, A., Shao, M., Wang, H., Wu, Y., Zeng, L., Hu, M., Kiendler-Scharr, A., Wahner, A., and Zhang, Y.: Wintertime photochemistry in Beijing: observations of ROx radical concentrations in the North China Plain during the BEST-ONE campaign, Atmospheric Chemistry and Physics, 18, 12391-12411, 2018.

Tang, M., Cziczo, D. J., and Grassian, V. H.: Interactions of Water with Mineral Dust Aerosol: Water Adsorption, Hygroscopicity, Cloud Condensation, and Ice Nucleation, Chemical Reviews, 2016.

Tang, M., Huang, X., Lu, K., Ge, M., Li, Y., Cheng, P., Zhu, T., Ding, A., Zhang, Y., Gligorovski, S., Song, W., Ding, X., Bi, X., and Wang, X.: Heterogeneous reactions of mineral dust aerosol: implications for tropospheric oxidation capacity, Atmospheric Chemistry and Physics, 17, 11727-11777, 2017.

Tang, M., Chan, C. K., Li, Y. J., Su, H., Ma, Q., Wu, Z., Zhang, G., Wang, Z., Ge, M., Hu, M., He, H., and Wang, X.: A review of experimental techniques for aerosol hygroscopicity studies, Atmospheric Chemistry and Physics, 19, 12631-12686, 2019.

Tao, J., Kuang, Y., Ma, N., Zheng, Y., Wiedensohler, A., and Zhao, C.: An improved parameterization scheme for size-resolved particle activation ratio and its application on comparison study of particle hygroscopicity measurements between HTDMA and DMA-CCNC, Atmospheric Environment, 226, 117403, 117410.111016/j.atmosenv.112020.117403, 2020.

Titos, G., Cazorla, A., Zieger, P., Andrews, E., Lyamani, H., Granados-Muñoz, M., Olmo, F., and Alados-Arboledas, L.: Effect of hygroscopic growth on the aerosol light-scattering coefficient: A review of measurements, techniques and error sources, Atmospheric Environment, 141, 494-507, 2016.

Twomey, S.: Measurements of natural cloud nuclei, Journal de Recherches Atmospheriques, 1, 101-105, 1963.

VanReken, T. M., Nenes, A., Flagan, R. C., and Seinfeld, J. H.: Concept for a new cloud condensation nucleus (CCN) spectrometer, Aerosol Science and Technology, 38, 639-654, 2004.

Voutilainen, A., Stratmann, F., and Kaipio, J. P.: A non-homogeneous regularization method for the estimation of narrow aerosol size distributions, Journal of Aerosol Science, 31, 1433-1445, 2000.

Wang, J., Shen, Y., Li, K., Gao, Y., Gao, H., and Yao, X.: Nucleation-mode particle pool and large increases in Ncn and Nccn observed over the northwestern Pacific Ocean in the spring of 2014, Atmospheric Chemistry and Physics, 19, 8845-8861, 2019a.

Wang, Q., Yang, S., Li, Y., Yin, Y., Zhang, Z., Chen, K., and Zhao, L.: A study of multi-size aerosol hygroscopic parameterization in the summer over Huangshan Mountain (in Chinese), Acta Meteorologica Sinica, 74, 989-1001, 2016.

Wang, T., Xue, L., Brimblecombe, P., Lam, Y. F., Li, L., and Zhang, L.: Ozone pollution in China: A review of concentrations, meteorological influences, chemical precursors, and effects, Science of the Total Environment, 575, 1582-1596, 2017a.

Wang, X., Ye, X., Chen, H., Chen, J., Yang, X., and Gross, D. S.: Online hygroscopicity and chemical measurement of urban aerosol in Shanghai, China, Atmospheric Environment, 95, 318-326, 2014.

1477 Wang, X., Shen, X. J., Sun, J. Y., Zhang, X. Y., Wang, Y. Q., Zhang, Y. M., Wang, P., Xia, C., Qi, X. F., and Zhong, J.
1478 T.: Size-resolved hygroscopic behavior of atmospheric aerosols during heavy aerosol pollution episodes in
1479 Beijing in December 2016, Atmospheric Environment, 194, 188-197, 2018a.
1480 Wang, X., Wang, X., and Yang, X.: Direct links between hygroscopicity and mixing state of ambient aerosols:
1481 Estimating particle hygroscopicity from their single particle mass spectra, Atmospheric Chemistry and Physics
1482 Discussions, 2020, 1-38, 2020a.
1483 Wang, Y., Wu, Z., and Hu, M.: Hygroscopicity of atmospheric sub-micrometer particles in various environments in
1484 China (in Chinese), China Environmental Science, 37, 1601-1609, 2017b.
1485 Wang, Y., Zhang, F., Li, Z., Tan, H., Xu, H., Ren, J., Zhao, J., Du, W., and Sun, Y.: Enhanced hydrophobicity and
1486 volatility of submicron aerosols under severe emission control conditions in Beijing, Atmospheric Chemistry and
1487 Physics, 17, 5239-5251, 2017c.
1488 Wang, Y., Li, Z., Zhang, Y., Du, W., Zhang, F., Tan, H., Xu, H., Fan, T., Jin, X., Fan, X., Dong, Z., Wang, Q., and Sun,
1489 Y.: Characterization of aerosol hygroscopicity, mixing state, and CCN activity at a suburban site in the central
1490 North China Plain, Atmospheric Chemistry and Physics, 18, 11739-11752, 2018b.
1491 Wang, Y., Wu, Z., Ma, N., Wu, Y., Zeng, L., Zhao, C., and Wiedensohler, A.: Statistical analysis and parameterization
1492 of the hygroscopic growth of the sub-micrometer urban background aerosol in Beijing, Atmospheric
1493 Environment, 175, 184-191, 2018c.
1494 Wang, Y., Li, Z., Zhang, R., Jin, X., Xu, W., Fan, X., Wu, H., Zhang, F., Sun, Y., Wang, Q., Cribb, M., and Hu, D.:
1495 Distinct Ultrafine- and Accumulation-Mode Particle Properties in Clean and Polluted Urban Environments,
1496 Geophysical Research Letters, 46, 10918-10925, 2019b.
1497 Wang, Y., Chen, Y., Wu, Z., Shang, D., Bian, Y., Du, Z., Schmitt, S. H., Su, R., Gkatzelis, G. I., Schlag, P., Hohaus, T.,
1498 Voliotis, A., Lu, K., Zeng, L., Zhao, C., Alfarra, M. R., McFiggans, G., Wiedensohler, A., Kiendler-Scharr, A.,
1499 Zhang, Y., and Hu, M.: Mutual promotion between aerosol particle liquid water and particulate nitrate
1500 enhancement leads to severe nitrate-dominated particulate matter pollution and low visibility, Atmospheric
1501 Chemistry and Physics, 20, 2161-2175, 2020b.
1502 Wiedensohler, A., Cheng, Y. F., Nowak, A., Wehner, B., Achtert, P., Berghof, M., Birmili, W., Wu, Z. J., Hu, M., Zhu,
1503 T., Takegawa, N., Kita, K., Kondo, Y., Lou, S. R., Hofzumahaus, A., Holland, F., Wahner, A., Gunthe, S. S., Rose,
1504 D., Su, H., and Poeschl, U.: Rapid aerosol particle growth and increase of cloud condensation nucleus activity
1505 by secondary aerosol formation and condensation: A case study for regional air pollution in northeastern China,
1506 Journal of Geophysical Research-Atmospheres, 114, D00G08, 10.1029/2008JD010884, 2009.
1507 Wu, Y., Yin, Y., Gu, X., and Tan, H.: An observational study of the hygroscopic properties of aerosols in north suburb
1508 of Nanjing (in Chinese), China Environmental Science, 34, 1938-1949, 2014.
1509 Wu, Y., Qiu, Y., Guo, J., Wang, K., Wang, J., and Zhou, X.: An Observational Study on the Hygroscopic Properties of
1510 Aerosol Particles at Different AltitudesA Case Study in the Mt. Huangshan (in Chinese), Resources and
1511 Environment in the Yangtze Basin, 27, 1361-1370, 2018a.
1512 Wu, Z., Zheng, J., Wang, Y., Shang, D., Du, Z., Zhang, Y., and Hu, M.: Chemical and physical properties of biomass
1513 burning aerosols and their CCN activity: A case study in Beijing, China, Science of the Total Environment, 579,
1514 1260-1268, 2017.
1515 Wu, Z., Chen, J., Wang, Y., Zhu, Y., Liu, Y., Yao, B., Zhang, Y., and Hu, M.: Interactions between water vapor and
1516 atmospheric aerosols have key roles in air quality and climate change, National Science Review, 5, 452-454,
1517 2018b.
1518 Wu, Z. J., Nowak, A., Poulain, L., Herrmann, H., and Wiedensohler, A.: Hygroscopic behavior of atmospherically
1519 relevant water-soluble carboxylic salts and their influence on the water uptake of ammonium sulfate, Atmospheric
1520 Chemistry and Physics, 11, 12617-12626, 2011.
1521 Wu, Z. J., Zheng, J., Shang, D. J., Du, Z. F., Wu, Y. S., Zeng, L. M., Wiedensohler, A., and Hu, M.: Particle
1522 hygroscopicity and its link to chemical composition in the urban atmosphere of Beijing, China, during
1523 summertime, Atmospheric Chemistry and Physics, 16, 1123-1138, 2016.
1524 Xie, Y., Ye, X., Ma, Z., Tao, Y., Wang, R., Zhang, C., Yang, X., Chen, J., and Chen, H.: Insight into winter haze
1525 formation mechanisms based on aerosol hygroscopicity and effective density measurements, Atmospheric
1526 Chemistry and Physics, 17, 7277-7290, 2017.
1527 Xu, B.: Hygroscopic properties of aerosol particles in Nanjing and Mount Huangshan (in Chinese), Master of Science,
1528 School of Atmospheric Physics, Nanjing University of Information Science and Technology, Nanjing, China, 31-
1529 45 pp., 2015.
1530 Xu, B., Zhang, Z.-f., Li, Y.-w., Qin, X., Miao, Q., and Shen, Y.: Hygroscopic Properties of Aerosol Particles in North
1531 Suburb of Nanjing in Spring (in Chinese), Huan jing ke xue= Huanjing kexue, 36, 1911-1918, 2015.

Yan, Y., Fu, P., Jing, B., Peng, C., Boreddy, S. K. R., Yang, F., Wei, L., Sun, Y., Wang, Z., and Ge, M.: Hygroscopic behavior of water-soluble matter in marine aerosols over the East China Sea, Science of the Total Environment, 578, 307-316, 2017.

Yang, F., Xue, H., Deng, Z., Zhao, C., and Zhang, Q.: A closure study of cloud condensation nuclei in the North China Plain using droplet kinetic condensational growth model, Atmospheric Chemistry and Physics, 12, 5399-5411, 2012.

Yang, S., Tian, Z., Zhang, T., Yu, X., Li, Y., An, J., Zhao, X., Li, Y., Wang, Z., and Wu, S.: Urban Aerosol Hygroscopicity During Haze Weather (in Chinese), Environmental Science, 40, 2546-2555, 2019.

Ye, X., Ma, Z., Hu, D., Yang, X., and Chen, J.: Size-resolved hygroscopicity of submicrometer urban aerosols in Shanghai during wintertime, Atmospheric Research, 99, 353-364, 2011.

Ye, X., Tang, C., Yin, Z., Chen, J., Ma, Z., Kong, L., Yang, X., Gao, W., and Geng, F.: Hygroscopic growth of urban aerosol particles during the 2009 Mirage-Shanghai Campaign, Atmospheric Environment, 64, 263-269, 2013.

Yeung, M. C., Lee, B. P., Li, Y. J., and Chan, C. K.: Simultaneous HTDMA and HR-ToF-AMS measurements at the HKUST Supersite in Hong Kong in 2011, Journal of Geophysical Research-Atmospheres, 119, 9864-9883, 2014.

Zhang, F., Li, Y., Li, Z., Sun, L., Li, R., Zhao, C., Wang, P., Sun, Y., Liu, X., Li, J., Li, P., Ren, G., and Fan, T.: Aerosol hygroscopicity and cloud condensation nuclei activity during the AC(3)Exp campaign: implications for cloud condensation nuclei parameterization, Atmospheric Chemistry and Physics, 14, 13423-13437, 2014.

Zhang, F., Li, Z., Li, Y., Sun, Y., Wang, Z., Li, P., Sun, L., Wang, P., Cribb, M., Zhao, C., Fan, T., Yang, X., and Wang, Q.: Impacts of organic aerosols and its oxidation level on CCN activity from measurement at a suburban site in China, Atmospheric Chemistry and Physics, 16, 5413-5425, 2016a.

Zhang, F., Wang, Y., Peng, J., Ren, J., Collins, D., Zhang, R., Sun, Y., Yang, X., and Li, Z.: Uncertainty in Predicting CCN Activity of Aged and Primary Aerosols, Journal of Geophysical Research-Atmospheres, 122, 11723-11736, 2017.

Zhang, F., Ren, J., Fan, T., Chen, L., Xu, W., Sun, Y., Zhang, R., Liu, J., Jiang, S., Jin, X., Wu, H., Li, S., Cribb, M. C., and Li, Z.: Significantly Enhanced Aerosol CCN Activity and Number Concentrations by Nucleation-Initiated Haze Events: A Case Study in Urban Beijing, Journal of Geophysical Research-Atmospheres, 124, 14102-14113, 2019a.

Zhang, J., Wang, L., Chen, J., Feng, S., Shen, J., and Jiao, L.: Hygroscopicity of ambient submicron particles in urban Hangzhou, China, Frontiers of Environmental Science & Engineering in China, 5, 342-347, 2011.

Zhang, Q., Meng, J., Quan, J., Gao, Y., Zhao, D., Chen, P., and He, H.: Impact of aerosol composition on cloud condensation nuclei activity, Atmospheric Chemistry and Physics, 12, 3783-3790, 2012.

Zhang, Q., Zheng, Y., Tong, D., Shao, M., Wang, S., Zhang, Y., Xu, X., Wang, J., He, H., Liu, W., Ding, Y., Lei, Y., Li, J., Wang, Z., Zhang, X., Wang, Y., Cheng, J., Liu, Y., Shi, Q., Yan, L., Geng, G., Hong, C., Li, M., Liu, F., Zheng, B., Cao, J., Ding, A., Gao, J., Fu, Q., Huo, J., Liu, B., Liu, Z., Yang, F., He, K., and Hao, J.: Drivers of improved PM2.5 air quality in China from 2013 to 2017, Proceedings of the National Academy of Sciences of the United States of America, 116, 24463-24469, 2019b.

Zhang, R., Wang, G., Guo, S., Zarnora, M. L., Ying, Q., Lin, Y., Wang, W., Hu, M., and Wang, Y.: Formation of Urban Fine Particulate Matter, Chemical Reviews, 115, 3803-3855, 2015.

Zhang, R., Tang, L., Xu, H., Du, S., Qin, W., Jiang, L., Tan, H., Liu, J., and Yang, Y.: Hygroscopic properties of urban aerosol in Nanjing during wintertime (in Chinese), Acta Scientiae Circumstantiae, 38, 32-40, 2018.

Zhang, S. L., Ma, N., Kecorius, S., Wang, P. C., Hu, M., Wang, Z. B., Groess, J., Wu, Z. J., and Wiedensohler, A.: Mixing state of atmospheric particles over the North China Plain, Atmospheric Environment, 125, 152-164, 2016b.

Zhang, X., Xu, X., Ding, Y., Liu, Y., Zhang, H., Wang, Y., and Zhong, J.: The impact of meteorological changes from 2013 to 2017 on PM2.5 mass reduction in key regions in China, Science China-Earth Sciences, 62, 1885-1902, 2019c.

Zhao, C., Yu, Y., Kuang, Y., Tao, J., and Zhao, G.: Recent Progress of Aerosol Light-scattering Enhancement Factor Studies in China, Advances in Atmospheric Sciences, 36, 1015-1026, 2019.

Zhu, T., Shang, J., and Zhao, D.: The roles of heterogeneous chemical processes in the formation of an air pollution complex and gray haze, Science China Chemistry, 54, 145-153, 2011.

Zhu, Y., Li, K., Shen, Y., Gao, Y., Liu, X., Yu, Y., Gao, H., and Yao, X.: New particle formation in the marine atmosphere during seven cruise campaigns, Atmospheric Chemistry and Physics, 19, 89-113, 2019.

Zieger, P., Vaisanen, O., Corbin, J. C., Partridge, D. G., Bastelberger, S., Mousavi-Fard, M., Rosati, B., Gysel, M., Krieger, U. K., Leck, C., Nenes, A., Riipinen, I., Virtanen, A., and Salter, M. E.: Revising the hygroscopicity of inorganic sea salt particles, Nature Communications, 8, 2017.